DYNAMIC TIDAL EFFECTS ON TSUNAMI COASTAL HAZARD IN LARGE ESTUARIES: CASE OF THE CHESAPEAKE BAY/JAMES RIVER, USA

BY

TAYEBEH S. TAJALLI-BAKHSH, STEPHAN T. GRILLI,

AND ANNETTE GRILLI

DEPT. OF OCEAN ENGINEERING
UNIVERSITY OF RHODE ISLAND

RESEARCH REPORT NO. CACR-15-09
DECEMBER 2015

SUPPORTED BY THE NATIONAL TSUNAMI HAZARD MITIGATION PROGRAM
NATIONAL WEATHER SERVICE GRANT NA14NWS4670041

CENTER FOR APPLIED COASTAL RESEARCH

Department of Civil and Environmental Engineering
University of Delaware
Newark, Delaware 19716, USA

Abstract

This work was performed as part of a tsunami inundation mapping activity carried out along the US East Coast since 2010, under the auspice of the National Tsunami Hazard Mitigation program (NTHMP). We develop tsunami inundation maps, in terms of envelopes of maximum flooding, by simulating coastal tsunami propagation for selected Maximum Probable Tsunamis (PMT) originated in the Atlantic ocean margin and basin. In the standard approach, tsunami simulations are performed over a static reference tide level, which is usually the Mean High Water (MHW) level (or for more critical facilities, the 10% exceedance tide level).

Our geographic area, however, features two main estuaries with significant tidal forcing, which are bordered by numerous critical facilities (power plants, major harbors,…) as well as densely built areas, located at low levels: the Hudson River Estuary and Chesapeake Bay (including the James River). In the present study, we apply a new methodology in which dynamic interactions between tide and tsunami are simulated to assess whether tidal effects lead to increased flooding as compared to the static level approach. The present report is limited to work done in Chesapeake Bay (CB), with a focus on the James River due to the location of a major Naval Base in Norfolk near its mouth and a nuclear powerplant (Surry) up the James River.

In our modeling methodology, we first separately simulate the dominant unscaled M2 tide and the two most significant incident tsunamis in the Atlantic Ocean Basin, on the continental shelf off of CB; this is done using the nonlinear and dispersive long wave model FUNWAVE-TVD, in coarse to medium nested grids. Then, the tide is calibrated in a finer grid encompassing the CB and the James river, in order to reproduce observations for the average tide and the selected maximum tide level (about MHW), at a tide gage located at the mouth of the James river near the Norfolk Naval Base. Combined tide-tsunami simulations are then performed, for a series of phases of the tides, by linearly superposing time series of surface elevation and horizontal currents of calibrated tide and tsunami wavetrains, along the offshore boundary of the CB grid, which is located on the shelf, in deep enough water for a linear approximation to be accurate. Combined tide-tsunami simulations are then performed with FUNWAVE-TVD, using the time series as boundary conditions; note these include both incident and reflected waves and thus satisfy an open boundary condition along the grid boundary.

Simulations are performed for incident tsunamis caused by an extreme Cumbre Vieja flank Collapse in the Canary Islands (volume of 450 km^3), and the historical Currituck slide on the continental shelf break, which is used as a local proxy for the maximum possible Submarine Mass Failure (SMF; see Grilli et al., 2015); 4 levels of nested grids are used, from 1 arc-min in the deep ocean down to a 39 m Cartesian grid in the James river. To identify the worst-case scenarios leading to maximum flooding, combined simulations are repeated for 4 different phases of the tide.

Results show that nonlinear interactions between tide and tsunamis affect the phase and elevation of tsunami wavetrains as they propagates up the estuary, as compared to a simple long wave superposition. However, most locations do not experience a significantly increased inundation level as compared to the static level simulations. More specifically, results show that the worst-case scenario, leading to maximum inundation and currents in the James River, is caused by the Cumbre Vieja tsunami, when combined with the extreme tide at one-eight of a period (about 1h 34 min) ahead of the maximum tide, along the grid offshore boundary. The Currituck slide tsunami causes nearly the same inundation for the same phase of the tide, although the wavetrains and current patterns in the river are very different. Depending on the arrival time of tsunami waves with respect to the tide phase, the major flooding risk in the river might result from different crests in the tsunami incident wavetrain and the arrival time of maximum flooding at a given location may vary. In all tide phase cases, nonlinear interactions between tide and tsunami currents change the velocity of propagation (phase speed) of various waves in the incident wavetrain, mostly in the shallower water area of the river where bottom friction dominates.

Overall, for all cases simulated, results show that the standard approach in tsunami hazard assessment, of simulating each tsunami over the maximum static extreme tide level produces conservative results in terms of maximum predicted inundation in the James River, but not by a large margin. It should be noted that, in the present case, maximum tidal currents are still moderate, less than 0.6 m/s in the river; clearly, in an estuary with stronger tidal currents, such as the Hudson River where currents can be more than double this speed, this conclusion could be reversed.

1. Introduction

Tides and tsunamis are both long waves, whose individual propagation is governed by long wave theories, such as linear Stokes theory in deep water and Saint Venant or Boussinesq equations in shallow water, depending on the relative magnitude of nonlinearity and dispersive effects (e.g., Dean and Dalrymple, 1990). In deep water, tsunamis are not affected by tides, because both the tidal range is small with respect to depth and tide-induced currents are weak. Hence, tsunami phase speed and shoaling are not significantly affected by the small change in water depth caused by tides and the current associated with the tsunami is usually stronger than tidal current. The same applies to shallow coastal waters with simple bathymetry and fairly straight coastlines. In this situation, which is prevalent for most of the ocean-exposed US east coast, from Florida to Massachusetts, while tide-induced currents may be larger and tidal range become more significant with respect to local depth, tsunami coastal hazard in terms of maximum inundation and runup can still be accurately assessed by modeling tsunami propagation using a static reference level corresponding to a large tide (typically the Mean High Water (MHW) or the 10% exceedence tide). In this case, both tsunami phase speed and elevation are properly affected by the increased depth, yielding larger inundation further onshore. However, in coastal regions where tidal range is large and/or the bathymetry is complex, and tide-induced flows can be strong, tsunami-tide interactions may need to be more carefully and accurately evaluated, in order to achieve a conservative coastal hazard assessment. This requires, in particular, considering whether nonlinear interactions between tidal and tsunami flow velocities and elevations may lead to more hazardous conditions. Along the US East Coast, significant tide-tsunami interactions could occur in a few large and complex estuaries, that are also be highly populated areas having numerous critical infrastructures (such as major harbors and powerplants), with prominent examples being New York, NY in the Hudson River estuary and Norfolk, VA near the mouth of the James River estuary in the Chesapeake Bay.

Since 2010, under the auspices of the US National Tsunami Hazard Mitigation Program (NTHMP; http://nthmp.tsunami.gov/index.html), the authors and co-workers from the University of Delaware, have been involved with modeling tsunami coastal hazard along the US East coast, including at these strongly tide-affected estuaries, under the effects of all the Probable Maximum Tsunamis (PMTs) that could occur in the Atlantic Ocean basin. These PMTs included (Fig. 1; see also ten Brink et al., 2008, 2014): (i) near-field submarine mass failures (SMFs) on or near the continental shelf break, represented in the Chesapeake Bay area by the historical Currituck (CRT) underwater landslide (Grilli et al. 2009; Grilli et al., 2013b; Grilli et al., 2015); (ii) an extreme hypothetical M9 seismic event occurring in the Puerto Rico Trench (Grilli et al., 2010; Grilli and Grilli, 2013a); (iii) a repeat of the historical 1755 M8.9 earthquake occurring in the Azores convergence zone (Madera Tore Rise; Barkan et al., 2009; Grilli and Grilli, 2013c); and (iv) a large scale flank collapse of the Cumbre Vieja Volcano (CVV) in the Canary Islands (Abadie et al., 2012; Grilli and Grilli, 2013b; Tehranirad et al., 2015). To carry out this tsunami inundation mapping work, a large number of tsunami simulations were performed using the fully

nonlinear and dispersive model FUNWAVE-TVD (Shi et al., 2012; Kirby et al., 2013), in a series of coarse to finer nested grids. According to the standard methodology, in the simulations, the reference level in the coastal grids was statically set to a high tide value (such as Mean Highest High Water Level; MHHWL). Hence, potential dynamic interactions between tide- and tsunami-induced flows were neglected.

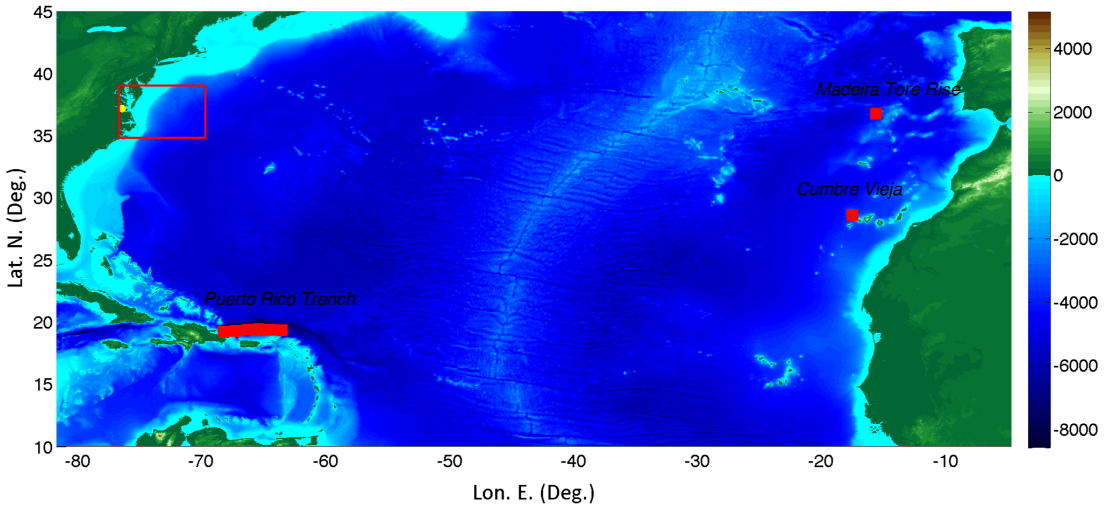

Fig. 1: Area of the 1 arc-min Atlantic Ocean basin grid (Table 1), with marked location of the three PMT far-field sources. The red box shows the footprint of 20 arc-sec (606 m) regional grid off of the Chesapeake Bay and the yellow dots marks the location of the James River. Color scale is bathymetry (< 0) and topography (> 0) in meter, from ETOPO-1 data.

To date, interactions between tide and tsunami waves have only rarely been studied. Kowalik et al. (2006) first hypothesized that significant effects due to tsunami–tide interactions should be observed in the tidal and tsunami currents. Kowalik and Proshutinsky (2010) modeled tide-tsunami interactions in a simple channel and then in Cook Inlet (Alaska), which has one of the largest tidal ranges in North America. They found that results significantly differed from a simple linear superposition of separate simulations of tide and tsunami, and that maximum elevations depended on the tide amplitude and phase; with tsunami being intensified or damped, depending on mean basin depth, which is regulated by tides. They concluded that, in their simulations, the main effects of the tide were to change water depth, thus affecting tsunami phase speed, propagation and amplification, and dissipation by bottom friction. These, however, were site specific conclusions and it is thus not possible to a priori predict the effects of tsunami–tide interactions without simulating tsunamis together with tidal forcing. Zhang et al. (2011) performed high resolution simulations of the impact of the 1964 Prince William Sound tsunami on the US Pacific Northwest coast, with and without dynamic tide effects. They evaluated the tidal influence on wave elevation, velocity and inundation. Their results showed that the tide, as could be expected, had minimal effects near the open coast, but significantly affected both wave runup and inundation near and in estuaries and rivers. On this basis, they concluded that dynamic tsunami–tide interactions should be considered in tsunami studies done near and in estuaries, as

these could account for 50% of the observed runup and up to 100% of the inundation in some cases. Tolkova (2012) and Yeh et al. (2012) modeled tsunami-tide interactions in the Columbia River (Oregon), to better understand the observed 100 km upstream propagation of the Tohoku 2011 tsunami in the river. Tolkova found that tsunami waves propagated further on a rising tide in the lower portion of the river; however, upstream the tsunami propagated further at the maximum high tide. The simulations performed also showed potential amplification of tsunami waves directly after high tide. Tolkova concluded that the interaction of the two long waves is completely dependent on the specific environment in which the interaction occurs, which justifies performing site-specific studies.

In this work, we first develop a methodology to simulate the combined effects of tidal phase and current magnitude on the evolution of tsunami waves, using FUNWAVE-TVD. With this method, we then model tsunami hazard in the Chesapeake Bay (CB) and James River estuary, in order to both gain insight into the nature of the combination and assess whether the resulting scenarios can potentially lead to more hazardous conditions than would be expected from a standard linear superposition of tide and tsunamis elevations. In the fairly shallow James River, tsunami phase speed and elevation are very dependent on local depth and direction of pre-existing current flows, which are both controlled by tide magnitude and phase. Additionally, large and sudden water level increases, such as those caused by an incoming tsunami elevation at the river mouth, may cause the appearance of a strongly dispersive and nonlinear undular bore, made of shorter oscillatory waves (e.g., Wei et al., 1995). The James River area was selected as the focused test bed for this work, because of the significant tide-induced flows, the complex topography and bathymetry both in the river and in the Chesapeake Bay (Figs. 2 and 3), and the many critical infrastructures that can be found in low lying areas of the river banks, including the largest Naval Base in the world, in Norfolk (VA) and the Surry nuclear power plant, halfway upstream the river (37°9′56″N, 76°41′52″W).

More specifically, we will evaluate tide-tsunami interaction effects by first simulating a representative large tide that can occur in the Chesapeake Bay and James River complex. Then, joint tide-tsunami simulations will be performed by superimposing incoming tsunami wave elevations and velocities with tidal forcing, along the offshore boundary of a computational grid selected where depth is large enough to justify their linear superposition. Tidal forcing will be limited to the strongest semi-diurnal component (M2), corresponding to the 10% exceedance tide on an average year, and will be obtained offshore from a tide simulation model. Regarding PMTs, the NTHMP work referred to above indicates that, in the case study area, among the 4 near- and far-field PMTs considered in the Atlantic Ocean, the two that by far are causing the largest waves at the mouth of the Chesapeake Bay are the CRT and CVV tsunamis. These two sources will thus be used as incident tsunamis to perform the tide-tsunami interaction study. Finally, effects of tide phase on the two incident tsunamis will be modeled by considering 4 different phases of the extreme M2 tide.

2. Modeling methodology

2.1 Tsunami propagation

Tsunami propagation is simulated using the fully nonlinear and dispersive Boussinesq model FUNWAVE (Wei et al., 1995; Grilli et al., 2007, 2010; Ioualalen et al., 2007), in its latest Cartesian (Shi et al., 2012a) and spherical (Kirby et al., 2013) implementations. FUNWAVE-TVD is fully parallelized for an efficient solution on shared memory clusters and has a more efficient Total Variation Diminishing (TVD) algorithm to follow breaking wave fronts in shallow water. The model has a quadratic bottom friction term controlled by a Manning friction coefficient C_d and, unlike the original FUNWAVE, it models dissipation in breaking waves by turning off dispersive terms in areas where breaking is detected based on a breaking index criterion. While FUNWAVE-TVD's Cartesian implementation is fully nonlinear, its spherical implementation is only mildly nonlinear; hence, it is only applicable in areas where tsunami elevation over local depth is perhaps not more than 10 percent. Therefore, in tsunami simulations, spherical grids will be fairly coarse and used to model large ocean areas in relatively deeper waters, whereas Cartesian grids will have a higher resolution and be used to model coastal tsunami impact. This approach was successfully used to model the Tohoku 2011 tsunami (Grilli et al., 2013a; Kirby et al., 2013). Both implementations of FUNWAVE-TVD have been fully validated against standard benchmarks, as part of the NTHMP work (Tehranirad et al., 2011; Shi et al., 2012b).

Simulations with FUNWAVE-TVD, whether spherical or Cartesian, are performed in several levels of nested grids using a one-way coupling methodology. This works by computing time series of free surface elevations and currents in a coarser grid level, for a large number of numerical gages (stations) defined along the boundary of the finer grid level. Computations in the finer nested grid level are then performed using these time series as boundary conditions. With this approach, reflected waves propagating from inside the area covered by each finer grid are included in the time series computed in the coarser grids along the finer grid boundaries, thus satisfying an open boundary condition. To reduce reflection in the first coarsest grid level (here the 1 arc-min Atlantic Ocean basin grid used to compute the transoceanic propagation of the CVV source; Fig. 1), 200 km thick sponge (absorbing) layers are specified along all the open boundaries.

Figures 1 to 3 show the footprints, locations, and bathymetry/topography of the FUNWAVE-TVD grids used in this work, i.e., a: (i) 1 arc-min (1800 m) resolution ocean basin spherical grid (Table 1); (ii) 20 arc-sec (606 m) resolution spherical regional grid (Table 2); and (iii) 154 m and 39 m Cartesian coastal grids (Tables 3 and 4). Tables 1-4 give details of the location and discretization of each grid. In each of those, bathymetry and topography are interpolated from the most accurate source available, i.e., 1 arc-min ETOPO-1 data in deeper water, 3 arc-sec (90 m) NOAA Coastal Relief model data (NOAA-NGDC, 2013), and 1/3 arc-sec (10 m) NTHMP or FEMA Region 3 Digital Elevation Models (DEMs; e.g., Taylor et al., 2008). Figs. 2 and 3 show

that the higher-resolution Cartesian grids used to better resolve the propagation of tsunami wave trains in the Chesapeake Bay and the James River, also accurately represent the complex geography and bathymetry of the region, despite only reaching a maximum resolution of 39 m, which is near the higher bound of typical resolutions used for inundation mapping (10-30 m), including the multiple deep and sometimes narrow channels.

Regarding reference levels, NOAA-NGDC's recommendation in deep water areas where ETOPO-1 bathymetry is used, is that tidal range should be neglected as it is within the error margin of the data. For computing tsunami inundation in coastal grids, however, using more accurate bathymetric data sources (such as the DEMs), the reference level should be adjusted to account for the high tides. In this work, however, rather than statically changing the reference level of tsunami simulations, dynamic tide-tsunami interactions will be simulated as detailed below.

2.2 Tsunami generation

As indicated above, based on earlier work, the two largest PMT sources selected for assessing tsunami coastal hazard in the Chesapeake Bay area are, in the far-field, an extreme 450 km^3 flank collapse of the Cumbre Vieja Volcano (CVV) in the Canary Islands (Abadie et al., 2012; Grilli and Grilli, 2013b; Tehranirad et al., 2015), and in the near-field a Submarine Mass Failure (SMF) identical to the Currituck slide (CRT), which is the largest historical SMF observed on the US Atlantic Ocean margin (Grilli et al., 2013b, 2015; ten Brink et al., 2008, 2014). Tsunami generation and resulting propagation from both of these sources have been studied in earlier work; hence, only a summary is given below and results are given in a following section.

Table 1: Parameters of the Atlantic Ocean basin model grid used for the CVV (450 km^3) far-field source definition and initial propagation modeling using FUNWAVE-TVD (Fig. 1).

Grid/Source	Min. Lon. E. (Deg.)	Max. Lon. E. (Deg.)	Min. Lat. N. (Deg.)	Max. Lat. N.(Deg.)	Resolution	Spherical /Cartesian
CVV 450 km^3	-82	-5	10	45	1 arc-min	Spherical

Table 2: Parameters of the 20 arc-sec regional grid used in FUNWAVE-TVD simulations (Fig. 2).

20 arc-sec/ "606 m" grid	Min	Max	Number of Cells	Cartesian/ spherical	Spatial Discretization (Deg.)	Center of Mercator Projection
Lat. (y)	34.8000	39.0167	760	Spherical	0.0056	34.8000
Lon. (x)	-77.0000	-69.9833	1264	Spherical	0.0056	-77

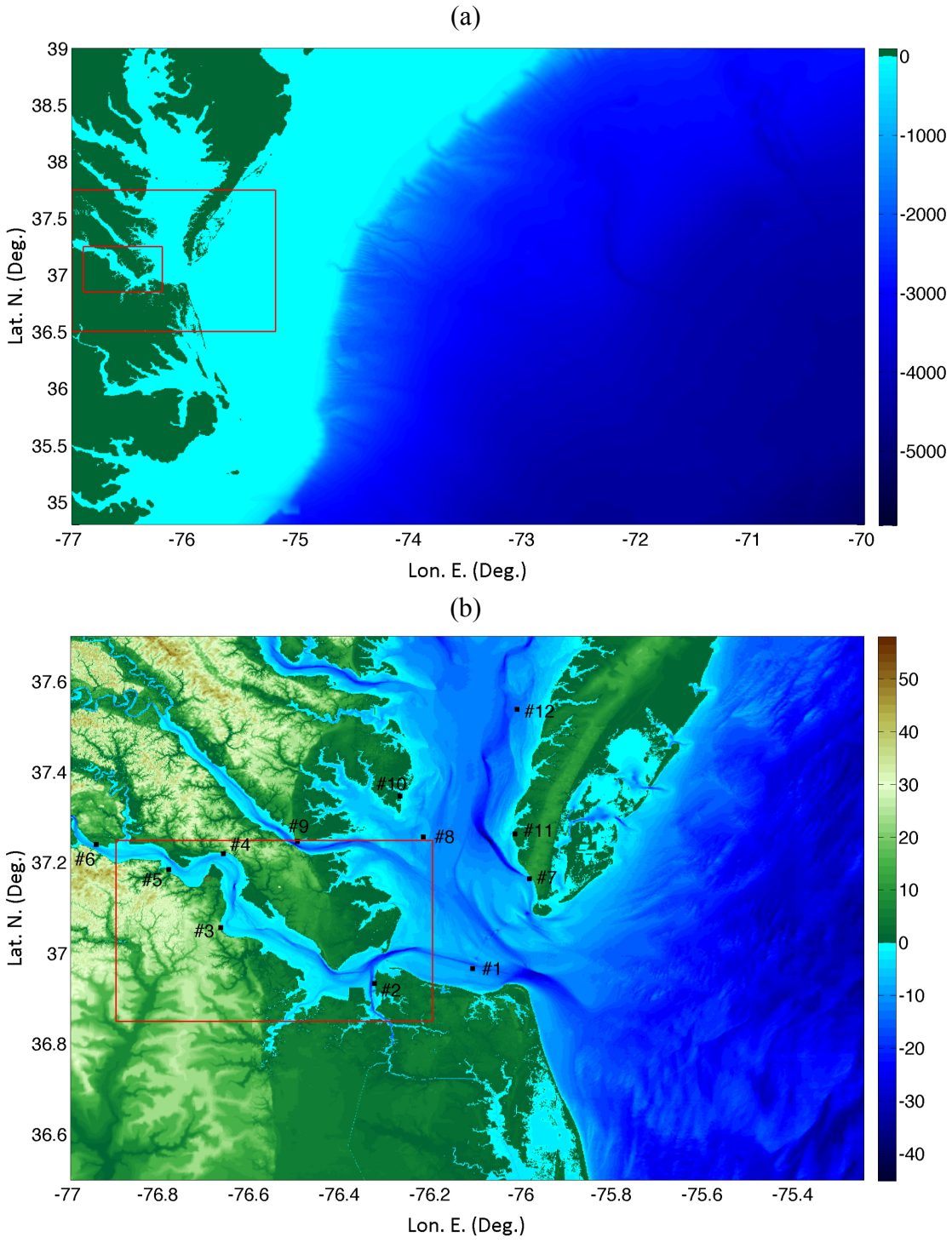

Fig. 2: Case study area and grids used in FUNWAVE-TVD simulations: (a) Chesapeake Bay and shelf in 20 arc-sec (606 m) spherical grid (Table 2). Bathymetry/topography (in meter) is from ETOPO-1. Red boxes mark the areas of the 154 m and 39 m nested grids; (b) Mouth of the Chesapeake Bay and James River Area in 154 m Cartesian grid (Table 3). Bathymetry/topography (in meter) is from 90 m CRM and 10 m NTHMP and FEMA DEMs (referred to MHW level). The red box marks the area of the 39 m nested Cartesian grid (Fig. 3) and black squares mark locations of NOAA tide gages #1-#12 (Table 5).

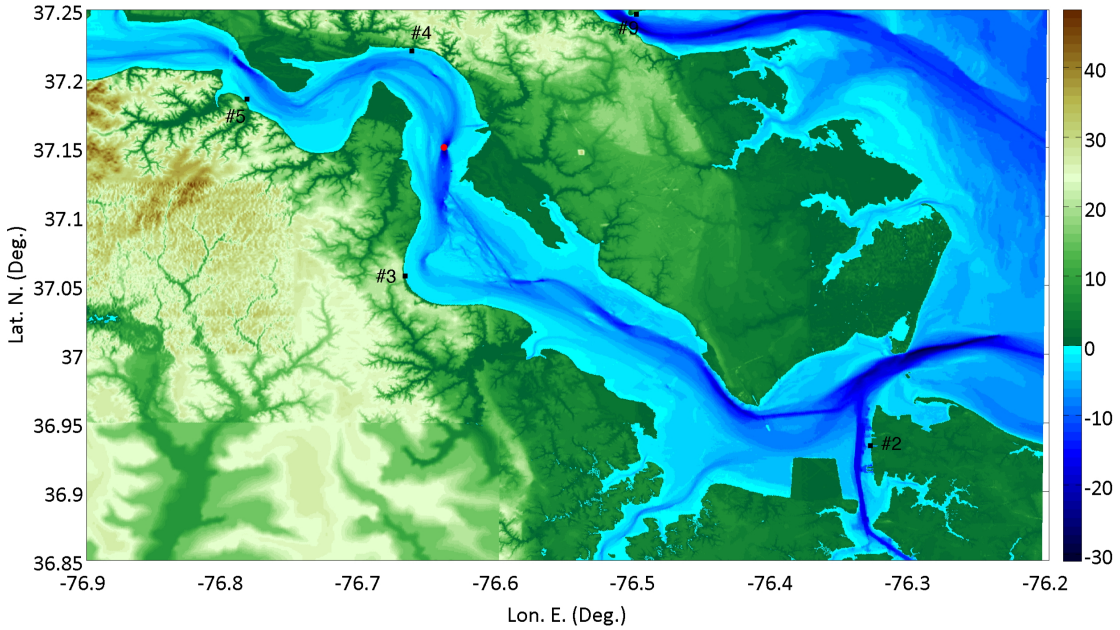

Fig. 3: James River in area of the 39 m Cartesian grid used in FUNWAVE-TVD simulations (Table 4). Bathymetry/topography (in meter) is from 10 m NTHMP and FEMA DEMs (referred to MHW level). The black boxes mark locations of NOAA tide gages (Table 5), and the red circle is the "river station".

Table 3: Parameters of the 154 m coastal grid used in FUNWAVE-TVD simulations (Figs. 2, 3).

"154 m" grid	Min	Max	Number of Cells	Cartesian/ spherical	Spatial Discretization (m)	Center of Mercator Projection
Latitude	36.5	37.7478	909	Cartesian	154.1227	36.5
Longitude	-77.0	-75.2016	1029	Cartesian	154.1227	-77.0

Table 4: Parameters of the 39 m coastal used in FUNWAVE-TVD simulations (Fig. 3).

"39 m" grid	Min	Max	Number of Cells	Cartesian/ spherical	Spatial Discretization (m)	Center of Mercator Projection
Latitude	36.8500	37.2495	1157	Cartesian	38.5307	36.8500
Longitude	-76.9000	-76.2014	1609	Cartesian	38.5307	-76.9000

CVV Flank collapse PMT: Earlier inundation mapping work performed for NTHMP indicated that the tsunami generated by a complete flank collapse of the Cumbre Vieja Volcano (CVV) on La Palma, in the Canary Islands, represents the largest far-field tsunami source that can potentially affect the US east coast (Abadie et al., 2012; Grilli and Grilli, 2013b; Tehranirad et al., 2015). Although the return period for this event is unknown and likely very long, it would generate such high waves that, even after transoceanic propagation, they would still pose a significant hazard to many coastal areas. The pioneering, but somewhat controversial, work of Ward and Day (2001) considered a CVV slide volume of 500 km^3, which they estimated would generate a tsunami causing 10 to 25 meter runup along the US East coast. More recent work,

based on more accurate modeling, predicted significantly smaller runup, although still very large in many areas (Abadie et al., 2012; Tehranirad et al., 2015). More specifically, Abadie et al. (2012) used the 3D multi-fluid Navier-Stokes model THETIS to compute several scenarios of CVV western flank collapse, with the most extreme having a 450 km^3 volume. In these simulations, in addition to water and air, the subaerial slide material was modeled as a Newtonian fluid having the density of basalt (2,500 kg/m^3). THETIS was used to compute both slide motion and tsunami generation, as well as near-field tsunami impact in and near La Palma. FUNWAVE-TVD was then used to simulate tsunami impact on the other Canary Islands, by initializing simulations with THETIS' solution. The surface elevation and current computed by Abadie et al., 20 minute into this event, have been used to define the extreme CVV source for assessing tsunami hazard along the US East Coast in NTHMP work (Grilli and Grilli, 2013b; Tehranirad et al., 2015). This was done by using this source as initial condition in a 1 arc-min FUNWAVE-TVD ocean basin scale grid, and performing further simulations in finer regional and coastal nested grids.

In this work, the propagation of the CVV tsunami will first be recomputed in a similar 1 arc-min ocean basin grid (Fig. 1; Table 1) to compute time series of surface elevation and current along the boundary of the 20 arc-min regional grid off of the Chesapeake Bay (Fig. 1).

CRT submarine mass failure PMT: Grilli et al. (2015) used the 3D non-hydrostatic sigma-layer model NHWAVE (Ma et al., 2012) to compute tsunami generation from the CRT-SMF motion. This model was validated for SMF tsunami simulations as part of NTHMP work (Tehranirad et al., 2012). To maximize tsunami generation, they used the total volume (165 km^3) of the reconstituted (unfailed) historical slide and assumed a failure as a rigid slump (Grilli and Watts, 2005; Enet and Grilli 2007). Once the SMF had stopped moving, 13.3 minutes into the event, the surface elevation and horizontal current were used as initial conditions in FUNWAVE-TVD to continue simulating tsunami propagation and coastal impact, in a series of nested grids.

In this work, the CRT tsunami propagation and coastal impact will be similarly computed by initializing FUNWAVE-TVD's computations in the 20 arc-sec grid (Fig. 2), using NHWAVE's solution at 13.3 min into the CRT event.

2.3 Tide-tsunami interactions

In earlier inundation mapping work performed for NTHMP, the static reference (or antecedent water) level used for coastal grids has been the local Mean High Water (MHW) level. However, according to the methodology established by the US Nuclear Regulatory Commission (NUREG/CR-6966), for critical coastal facilities such as nuclear powerplant, tsunami runup and inundation should be evaluated coincidentally with an antecedent water level (AWL) equal to the 10% exceedance high tide, defined as the tide that is equaled or exceeded by 10% of the maximum monthly tides over a continuous 21 year period (ANSI/ANS-2.8-1992), which is usually higher than the MHW level. Additionally, the AWL should include a water level

increase due to sea level rise (SLR). The main innovation in this work is to assess coastal tsunami hazard by considering dynamic interactions between tsunami flows and a tide calibrated to achieve a specified maximum AWL, rather than using this AWL as a high water reference static level throughout tsunami simulations. To perform this comparison, in preliminary tide-only simulations, tidal forcing will be calibrated for the maximum dynamic tide elevation to still achieve AWL conditions at a selected reference point.

Since the focus of this tsunami hazard assessment is the James River, the AWL was calculated using tide data obtained at NOAA's Sewells Point, VA, gage (NOAA Station 8638610; marked #2 in Figs. 2, 3; Lat. 36° 56.8', Lon. 76° 19.8'), which is near the river mouth. This yields, 0.945 m NAVD88 for the 10% exceedance tide maximum elevation and 0.287 m NAVD88 for the MHW (Mean Sea Level (MSL) is 0.079 m below NAVD88); according to a standard scenario we find 0.299 m for SLR; hence the conservative AWL is 1.244 m NAVD88. Additionally, the dominant tidal constituent at Sewells Point is clearly the M2 (semi-diurnal) tide, since it is nearly five times greater than the next two constituents (N2 and S2). Therefore, the M2 tide constituents will be considered as representative of the general tidal conditions in the Chesapeake Bay and the James River.

As indicated before, in deep enough water with respect to surface elevation, both tide and tsunami waves behave as nearly linear long waves. Accordingly, when these conditions are met, linear wave theory's superposition principle (Dean and Dalrymple, 1990) applies and their surface elevation and current can be added. Here, the 154 m grid (Fig. 2) was designed such that its (eastern) offshore boundary is mostly located in a 20-30 m depth, where the linear approximation is deemed to apply in view of the small or moderate elevation of incident tsunamis and tide along this boundary. In view of this, the methodology used for simulating tide-tsunami interactions with FUNWAVE-TVD in the James River will be to: (i) obtain the unscaled tide components along the boundary of the 154 m grid from a regional tide model; (ii) perform tide only simulations in the 154 m grid using (i) as boundary condition, for a reference level equal to MHW + SLR = 0.586 m NAVD88; (iii) in a few iterative simulations, calibrate the boundary forcing to obtain the expected AWL at Sewells Point, as well as realistic elevations at the other stations in the James River (#3-#5; Fig. 2); (iv) perform tsunami simulations for each of the 2 selected PMTs (CRT and CVV), to obtain incident tsunami time series of elevation and current along the boundary of the 154 m grid; (v) perform joint tide-tsunami simulations in the 154 m grid, forced by the superimposition of tidal forcing (for a few selected phases) and each incident tsunami wave train along its boundary, and initialized with results of the calibrated tide only simulation; compute time series of the joint tide-tsunami solution along the boundary of the 39 m grid (Fig. 2); and (vi) perform joint tide-tsunami simulations in the 39 m grid forced by time series along its boundary, and initialized with results of the calibrated tide only simulation.

In this work, the M2 tidal constituents were obtained from OSU's Regional Tidal Solution for the East Coast of America (Egbert et al, 1994, 2002), as unscaled surface elevation and horizontal velocity data, interpolated at the coordinates of all the boundary points of the 154 m

grid. Due to the slow quasi-sinusoidal variation of the M2 tide over its 12.42 hour period (44,712 s), a large time step of 1,863 s (31 min) was used to create M2 tide time series; these, however, were then re-interpolated for the actual time steps used by FUNWAVE-TVD. Because of the periodicity, any time step can be used as the first step, allowing the incident tsunamis to be synchronized with various phases of the tides.

The joint tide-tsunami simulations start with the arrival of the first crest (usually the highest one) in each tsunami wave train at the (eastern) offshore boundary of the 154 m grid (Fig. 2). When this happens, a given phase of the tide is assumed to occur on the boundary, leading to a specific time lag in the tide boundary time series, before linearly superimposing them with the tsunami time series; both surface elevation and current computed at this time in the tide-only simulations will be used as initial condition in the 154 m domain.

Because both tide and tsunami are long waves, to the first-order, they propagate at the same phase speed in the CB and the James River, so the selected combination of tide and tsunami elevations at the boundary should be preserved up the James River except for nonlinear effects. Nonlinear effects, indeed, will make the tide and tsunami flows interact and modify their respective propagation; modeling these effects to see whether this can potentially lead to more hazardous conditions (i.e., inundation and currents) is the object of this work. To do so, the tide-tsunami superposition will consider 4 different phases of the tide, at the middle of the eastern boundary of the 154 m grid (there will be small spatial variations of the tide along the boundary): (1) maximum tide; (2) T/8 after maximum tide; (3) T/4 after maximum tide (i.e., downward zero crossing tide), and (4) T/8 ahead of maximum tide. The case of a rising tide was a priori eliminated here because it was thought that, in a friction dominated environment such as the James River estuary, the superposition of co-flowing tide and tsunami currents would increase bottom friction dissipation and hence reduce the combined elevation. By contrast, a tsunami moving into an ebbing tide would have a relatively smaller current, causing less bottom friction dissipation and creating a blockage situation that could increase surface elevation.

Because tsunami and tide elevations in the James River are strongly affected by bottom friction, one must use a realistic friction coefficient value. Data, however, is lacking in this respect and we will thus use the typical value for coarse sand, which is prevalent in the region, $C_d = 0.0025$. This is the same value as used in the NTHMP work to model tsunami inundation on typical beaches (such as for nearby Virginia beach). Tide data is available in the CB and James River for 12 NOAA stations; hence, in the calibration of the tide-only simulations, we will verify that given this friction coefficient, simulations of average tides are in good agreement with field data.

3. Modeling of incident tsunami sources

3.1 Modeling of near-field CRT-SMF source

Tsunami generation from the near-field Currituck SMF (CRT; Fig. 4) is simulated with the 3D model NHWAVE, using space and time varying bottom boundary conditions, calculated from

the SMF geometry and kinematics. The latter are expressed using Grilli and Watts' (2005) and Enet and Grilli's (2007) approach, assuming a rigid slump motion, based on the CRT-SMF parameters: length b = 30 km, width w = 20 km, thickness T = 0.75 km, slope angle 4 deg., direction of failure due east, and center of the SMF located at 74.61W and 36.39N. This yields a SMF runout of s_f = 15.8 km and a failure time of motion of t_f = 710 s (11.8 min.); details can be found in Grilli et al. (2015). Using this kinematics NHWAVE simulations are performed in a 3D grid made of a 500 meter resolution horizontal Cartesian grid (Fig. 4) and 3 sigma layers in the vertical direction. This yields the surface elevation shown in Fig. 3b at t = 13.3 min., after the SMF has stopped moving, which is identical to that found in earlier NTHMP work (Grilli et al. 2013b, 2015); at this time, surface elevation ranges between -20 and +20 m. The CRT tsunami simulations are pursued in FUNWAVE-TVD by re-interpolating the SMF source at 13.3 min. onto the 20 arc-sec grid. Note that sensitivity analyses performed

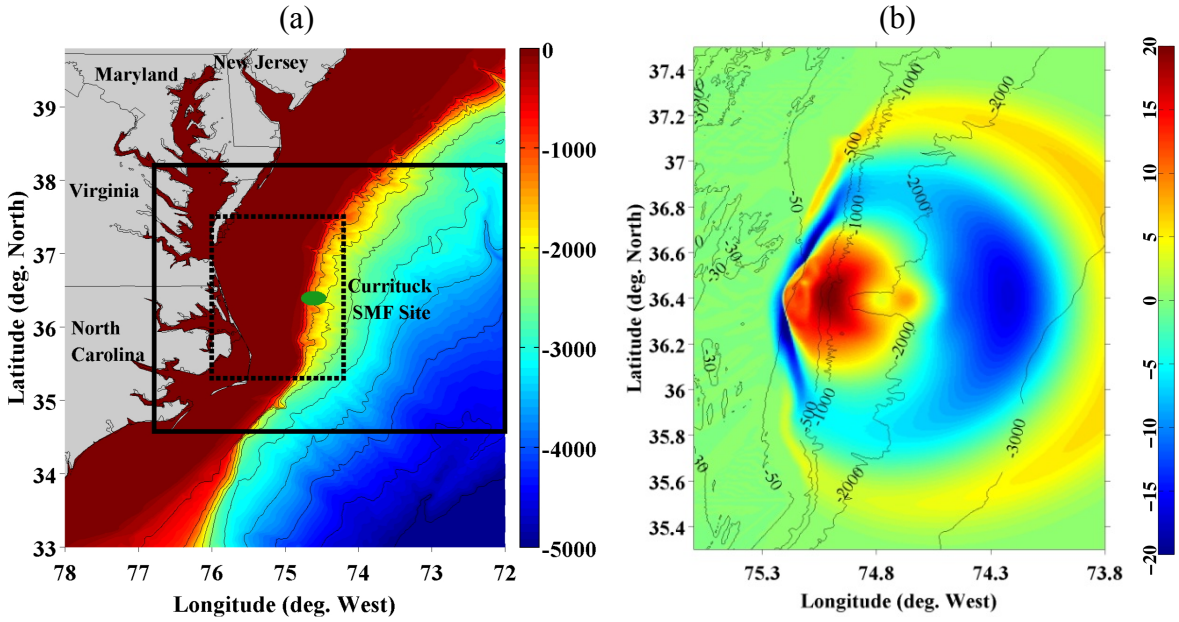

Fig. 4: (a) Area of the historical Currituck SMF (green ellipse is the footprint of the unfailed SMF centered at 74.61W and 36.39N), with depth in meter in the color scale. The solid black box marks the boundary of a 500 m resolution grid used in NHWAVE simulations (3 sigma-layers) to compute the SMF tsunami source up to 13.3 min. after triggering; and (b) surface elevation (color scale is in meter) computed at 13.3 min. with NHWAVE, shown in the dashed box of plot (a). Bathymetric contours are marked in meter. [From Grilli et al. (2013b, 2015).]

Figure 5a shows the surface elevation at 13.3 min. re-interpolated in the 20 arc-sec grid, and Figs. 5b and 5c show surface elevations computed with FUNWAVE-TVD at 34 min and 1h 10 min., respectively, after SMF triggering. At the latter time, large elevation and depression waves, nearly +5 m and -4 m, respectively, are seen to propagate towards the mouth of Chesapeake Bay and even larger waves are heading for the coast of Virginia Beach, VA and south of it. [Note, in Fig. 5c, south and north of the grid, there are slight artifacts caused by the sponge layers; these do not affect results in the area of interest near the Chesapeake Bay mouth.] The large size of

waves heading for the coast is confirmed in Fig. 6, which shows the envelope of maximum surface elevations computed between 30 min. and 6h 15 min. (where the initial time is selected to eliminate the large waves near the source that would make the figure less readable). The incident wave train of the CRT-SMF tsunami is shown in Fig. 7. At the southeast corner of the 154 m grid (-77.2E, 36.5N), a very large elevation wave of about 9 m is seen to be heading for the coast south of Virginia. This is a location directly west of the Currituck failure, which is east-west oriented and has a center at 36.39N (Fig. 4a), where the largest waves are expected to be found. Further north, east of the Chesapeake Bay mouth (-75.2E, 37.15N), the incident wave train has two leading waves, reaching up to +4 m, with a minimum of -4 m. Using such tsunami time series as boundary conditions, computations will be pursued by one-way coupling in 2 more levels of nested Cartesian grids (154 and 39 m; Figs. 2 and 3), in combination with tidal forcing. This is detailed later.

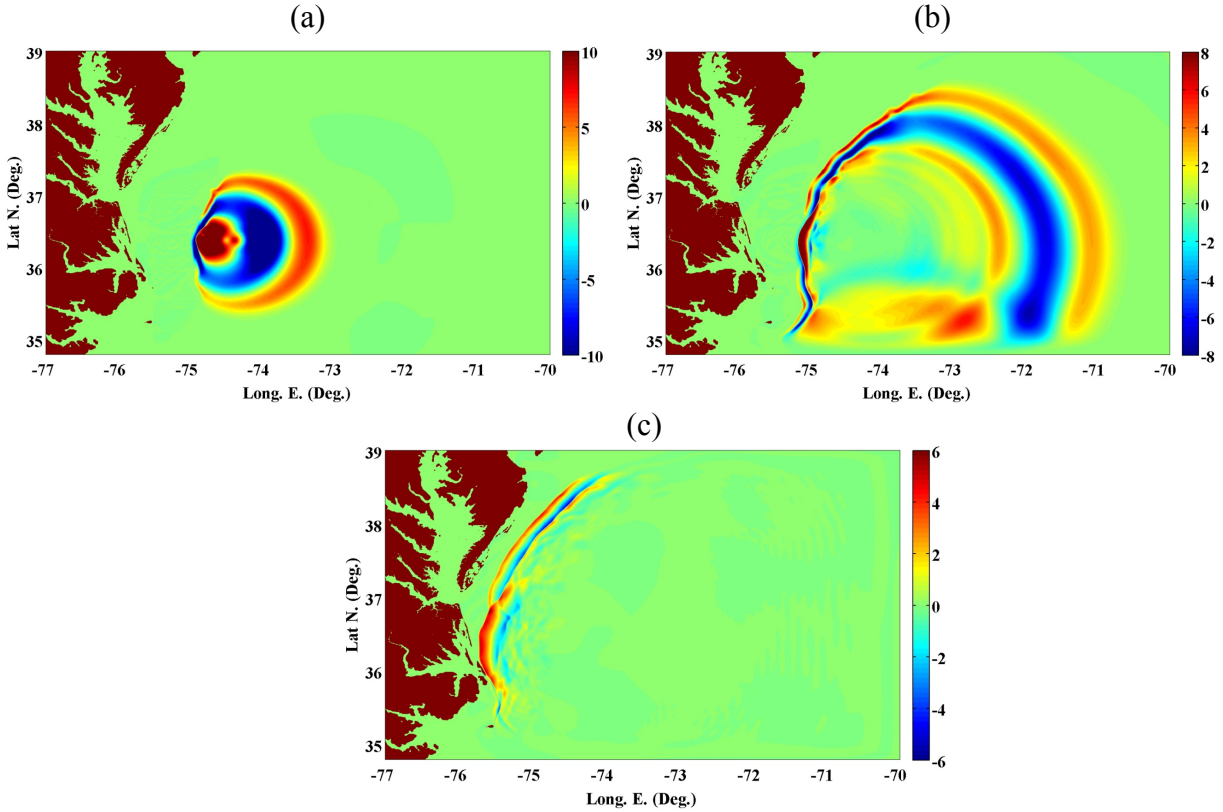

Fig. 5: FUNWAVE-TVD simulations of the CRT-SMF tsunami in the 20 arc-sec grid (Fig. 2; Table 2). Surface elevation computed at *t* = (a) 13.3 min.; (b) 34 min.; and (c) 1h10 min., after SMF triggering. Color scale is in meter.

3.2 Modeling of far-field CVV source

In accordance with earlier NTHMP studies (Grilli and Grilli, 2013b; Tehranirad et al., 2105), FUNWAVE-TVD is used to compute the transoceanic propagation of Abadie et al.'s 450 km^3 CVV collapse scenario, in the 1 arc-min ocean basin grid (Fig. 1; Table 1). The model is

initialized from the surface elevation and horizontal velocity computed with THETIS at 20 min. into the event (Fig. 8). Computations are pursued by one-way coupling in the 20 arc-sec resolu-

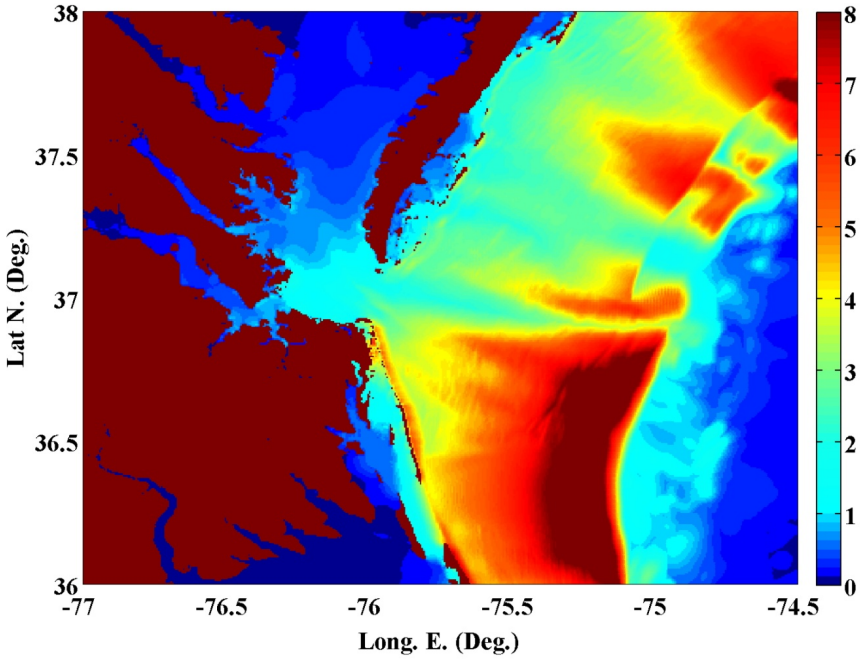

Fig. 6: Maximum envelope of surface elevation (color scale in meter) in FUNWAVE-TVD simulations of the CRT-SMF tsunami, in a zoom-in of the 20 arc-sec grid (Fig. 2; Table 2), from 30 min. up to 6h 15 min. of propagation.

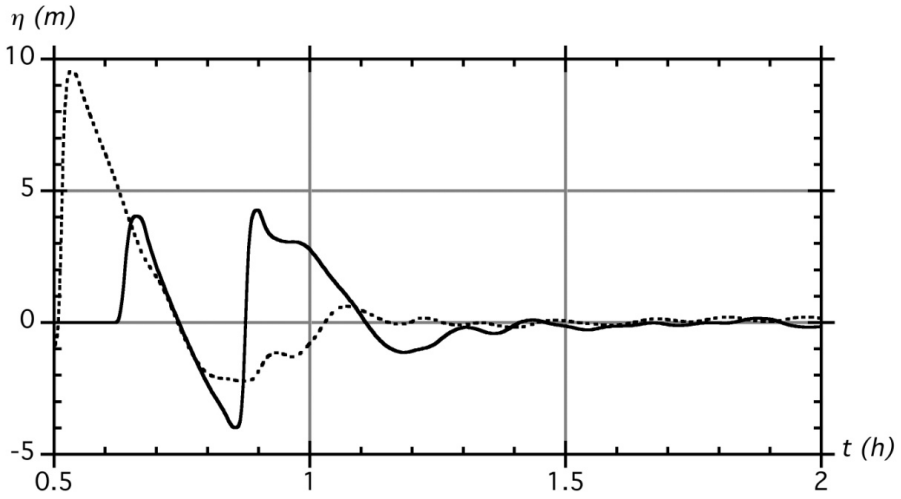

Fig. 7: FUNWAVE-TVD simulations of the CRT-SMF in 20 arc-sec FUNWAVE grid (Fig. 2, Table 2). Time series of surface elevation computed at the 154 m grid (Table 3): (dash line) southeast corner (36.5N; -75.2E); (solid line) middle of eastern boundary, in front of the Chesapeake Bay mouth (37.15N; -75.2E).

tion grid (Figs. 1 and 2). Figure 9 shows the instantaneous surface elevation computed in this grid at 8h 20 min and 9h 20 min after the start of the event, and Fig. 10 shows the envelope of

maximum surface elevation computed up to 9h 20 min. We see that large elevations of up to 9 m occur off the shelf, east of the Chesapeake Bay mouth; but owing to dissipation over the wide shelf (essentially bottom friction as shown in Tehranirad et al., 2015), elevations are reduced to 6 m closer to the Bay mouth, consistent with earlier work (Grilli and Grilli, 2013b; Tehranirad et al., 2015). These large waves are confirmed by the time series of surface elevation shown in Fig. 11, at the southeast corner of the 154 m grid; we also see the highly dispersive nature of the incident wave train. Using such time series as boundary conditions, computations are then pursued by one-way coupling in 2 more levels of nested Cartesian grids (154 and 39 m; Figs. 2 and 3), in combination with tidal forcing. This is detailed later.

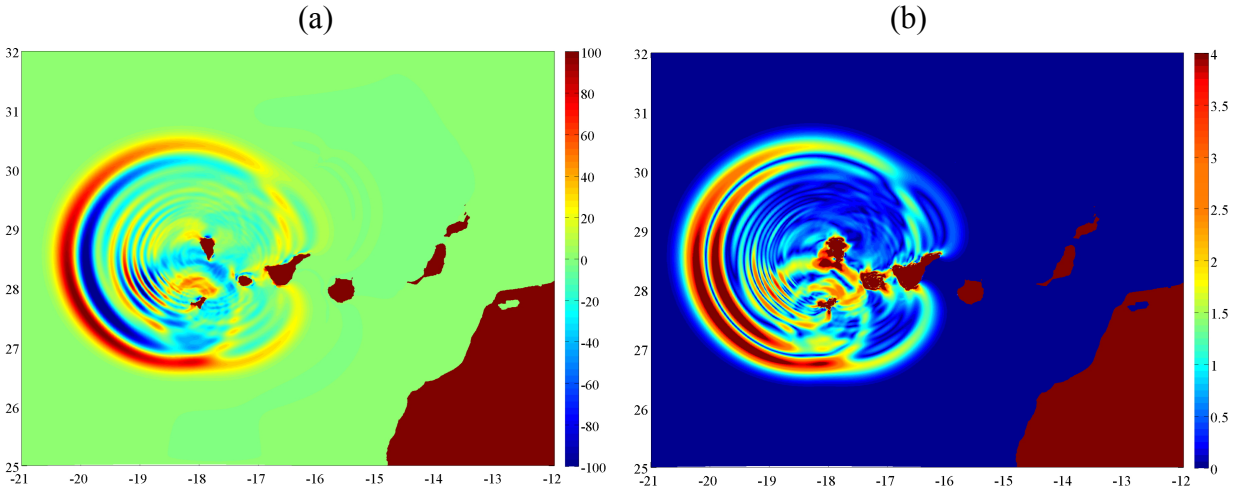

Fig. 8. (a) Initial surface elevation (color scale in meter), and (b) module of the horizontal velocity (color scale in meter/second), at 20 minutes after the start of the event, for Abadie et al.'s (2012) 450 km^3 CVV subaerial landslide source.

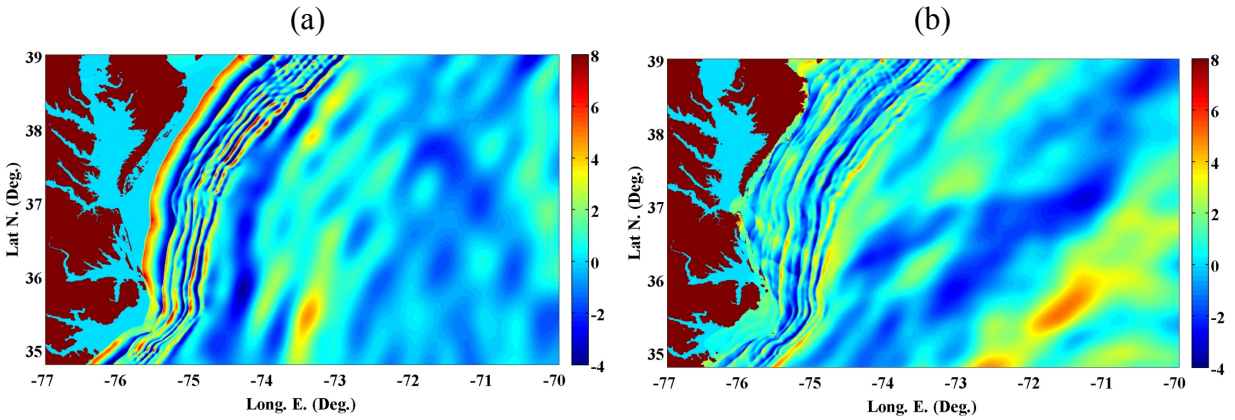

Fig. 9. Surface elevation (color scale in meter) computed at t = (a) 8h 20 min.; and (b) 9h 20 min., in FUNWAVE-TVD simulation of the 450 km^3 CVV flank collapse in 20 arc-sec grid (Figs. 1, 2; Table 2).

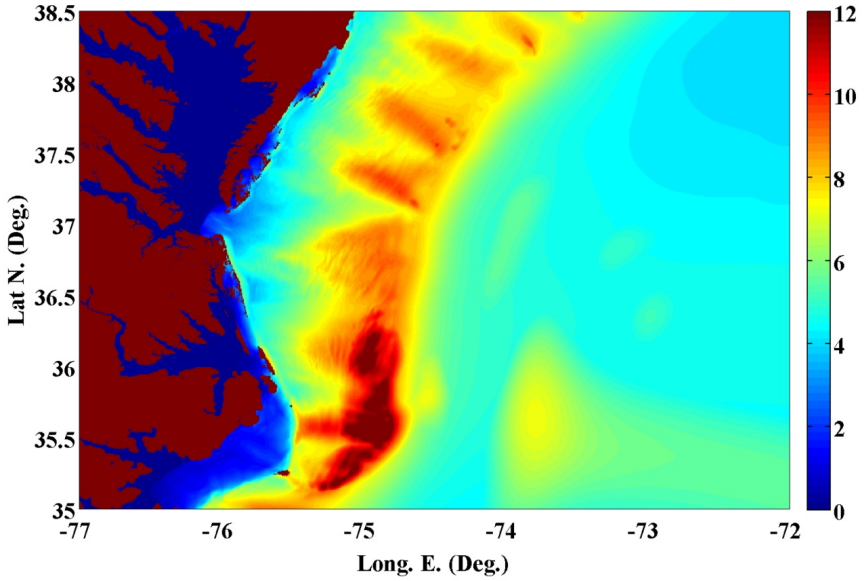

Fig. 10: Envelope of maximum surface elevation (color scale in meter) computed up to 9h 20 min., in FUNWAVE-TVD simulation of the 450 km^3 CVV flank collapse in zoom-in of 20 arc-sec grid (Figs. 1, 2; Table 2).

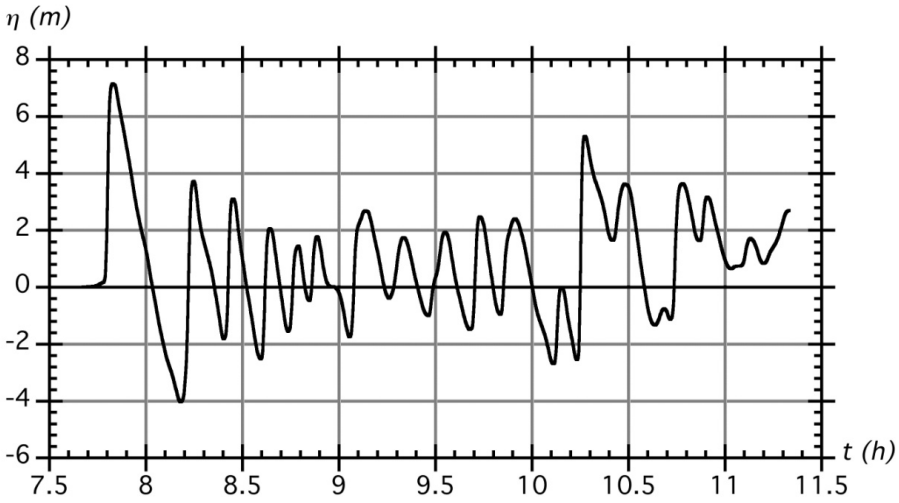

Fig. 11: Time series of surface elevation computed in FUNWAVE-TVD simulation of the 450 km^3 CVV flank collapse in the 20 arc-sec grid (Figs. 1 and 2; Table 2), at the 154 m grid south-east corner (Table 3).

4. Modeling and calibrating the extreme tide

We simulate the M2 tide with FUNWAVE-TVD in the 154 m resolution grid (Fig. 2; Table 3) and calibrate it to achieve the AWL at the Sewells Point tide gage, at the mouth of the James River (station #2 in Figs. 2). The unscaled M2 tide was obtained from the "OTIS Regional Tidal Solution: East Coast of America" (OSU Tidal Prediction Software, version 2beta (OTPS2), at 2 arc-min resolution), as time series of one tidal period (12.42 h or 44,712 s) of surface elevation and horizontal current, directly interpolated at the locations of the 154 m grid boundary nodes, to be used as boundary conditions. In FUNWAVE-TVD, time step is a function of grid size and

wave celerity c to achieve a mesh Courant number of about 0.5; thus, in the 154 m grid, where maximum depth is about h_{max} = 45 m (Fig. 2) and $c_{max} = (g\, h_{max})^{1/2}$ = 21.2 m/s, time step is ~ 3.6 s. The tide time series were interpolated to provide forcing values at each of these time steps.

The unscaled M2 tide is the mean tide, so this data is used as boundary forcing in a first simulation to verify the agreement of numerical results with mean tidal ranges measured at 12 NOAA tidal stations in the Chesapeake Bay and the James River (Fig. 2; Table 5; http://tidesandcurrents.noaa.gov/stations.html?type=Water+Levels). Then, based on results obtained at Sewells Point (station #2) in this simulation, the tidal forcing along the grid boundary is scaled up by a constant to achieve the expected AWL at Sewells Points. A second simulation is then performed using the scaled up tidal forcing, where it is verified that the AWL is indeed achieved at Sewells Point and corresponding maximum elevations in the James River are adequate for hazard assessment.

Because computations of tides with FUNWAVE-TVD are cold starts, to achieve a quasi-periodicity in the simulations, two full tidal periods will be simulated, plus a quarter period during which tidal forcing (both surface elevation and current) is gradually ramped-up along the 154 m grid offshore boundary (east, north and south) and northern boundary within the Bay (Fig. 2). Specifically, the tide time series were first shifted in time for the forcing to start with a rising tide (from zero level) near the middle and off of the Chesapeake Bay mouth, along the 154 m eastern boundary. However, because of small spatial phase shifts in the tide along the grid boundary, to have all the station time series starting from a zero surface elevation (and current) at the beginning of the simulation (thus ensuring model stability), a ramp-up was applied for the first quarter period of the M2 tide, or 3h 6 min., in the form of a "tanh" multiplier function varying between 0 and 1 over this interval. Hence, the total tide simulations lasted for 2.25 periods or 100,602 s (~28h).

4.1 Reference level in simulations

Before performing the tide simulations with FUNWAVE-TVD, one needs establishing, which reference level should be used. The 154 m grid bathymetry shown in Fig. 2 is referenced to MHW, which at Sewell Point is 0.287 m NAVD88, implying that the AWL, which is 1.244 m NAVD88, is 0.957 m above MHW; this values includes 0.299 m of sea level rise (SLR) and thus the 10% exceedence tide elevation should be an additional 0.658 m at Sewells Point.

While the logical choice for a reference level might a priori be Mean Sea Level (MSL), which at Sewells Point is -0.079 NAVD88, plus SLR in the present case, there are many uncertainties in surface elevation damping in the model, during tide propagation up the James River (e.g., in relation to bottom friction and grid resolution) as well as other uncertainties in the actual mean sea level associated with the occurrence of an extreme tide elevation (such as the 10% exceedence tide). Therefore, owing to the small difference between MSL and MHW (0.366 m) at Sewells Point, and in view of these uncertainties, for simulating inundation in the James River as a result of the combination of extreme tides and tsunamis, it was deemed more conservative calibrating the dynamic tidal forcing to achieve the AWL at Sewells Point, using MHW plus

SLR as the reference level (i.e., +0.586 m NAVD88); this means adding SLR to the current bathymetry. A comparison of numerical results to actual measurements at NOAA tide gages for the mean tide, as well as other targeted simulations using MSL plus SLR reference level, were conducted that confirmed the relevance of this choice (see details below).

4.2 Mean M2 tide simulation

We first simulate the mean M2 tide in the 154 m grid, with the depth referenced to MHW+SLR, using the mean (unscaled) M2 tide data as boundary condition. Figure 12a thus shows the envelope of maximum surface elevations computed for 2.25 periods of tidal forcing and corresponding time series of surface elevation are plotted in Fig. 13a, for NOAA stations #1-6 in the James River. Table 5 compares maximum minus minimum computed surface elevations and their phases at the 12 NOAA stations (Fig. 2) to measured tidal ranges and phases provided by NOAA. Overall, errors on tidal range are reasonably small, with the RMS of the relative error for the 12 gauges being 8%. Errors on phases of maximum tides are similarly reasonably small. More specifically, however, while the maximum level is overpredicted in the simulation at stations #1 and #2, near the mouth of the Bay and at Sewells Pt., respectively, when going up the James River, the maximum tide elevation is gradually underpredicted at stations #3 to #6. This over- then under-prediction justifies using a slightly higher reference level in these simulations (i.e., MHW+SLR instead of MSL+SLR), to achieve a maximum level in the James River closer to the expected value of the AWL, when the scaled M2 tide forcing will be used. This will be seen next.

4.3 Extreme M2 tide simulation

Simulations are run in the 154 m grid using a scale up tidal forcing on its boundary, to achieve AWL at Sewells Point, which requires a maximum tide elevation of 0.66 m when using MHW+SLR as a reference level. In Table 5, we see that the tide elevation is 0.41 m at this location, when forcing the simulation with the mean tide. Hence, based on these results the calibration factor to scale up the tidal forcing should be about 0.66/0.41 = 1.61. Because of nonlinear effects in tide propagation (including bottom friction which is enhanced for larger tides), however, a couple of iterations of simulations were necessary to eventually find the calibration of 1.9 that allows achieving the AWL at Sewells Point. The envelope of maximum surface elevation obtained for this scaling is plotted in Fig. 12b and corresponding time series of surface elevation are plotted in Fig. 13b, for NOAA stations #1-6 in the James River. In the latter, the time series of surface elevation at Sewells Point (gages #2), confirms that the maximum tide level reaches 0.66 m above MHW+SLR. Further upstream the James River, at station #4, the maximum tide elevation reaches 0.58 m, which is 0.08 m below the maximum elevation at Sewells Point. This is entirely consistent with NOAA's data for mean tide levels listed in Table 5, where the maximum elevation in station #4 is 0.04 m less than that in station #2, yielding 0.076 m after scaling up by a factor 1.9. These results further confirm the relevance of using MHW+SLR as a reference level in simulations aimed at calibrating the extreme tide.

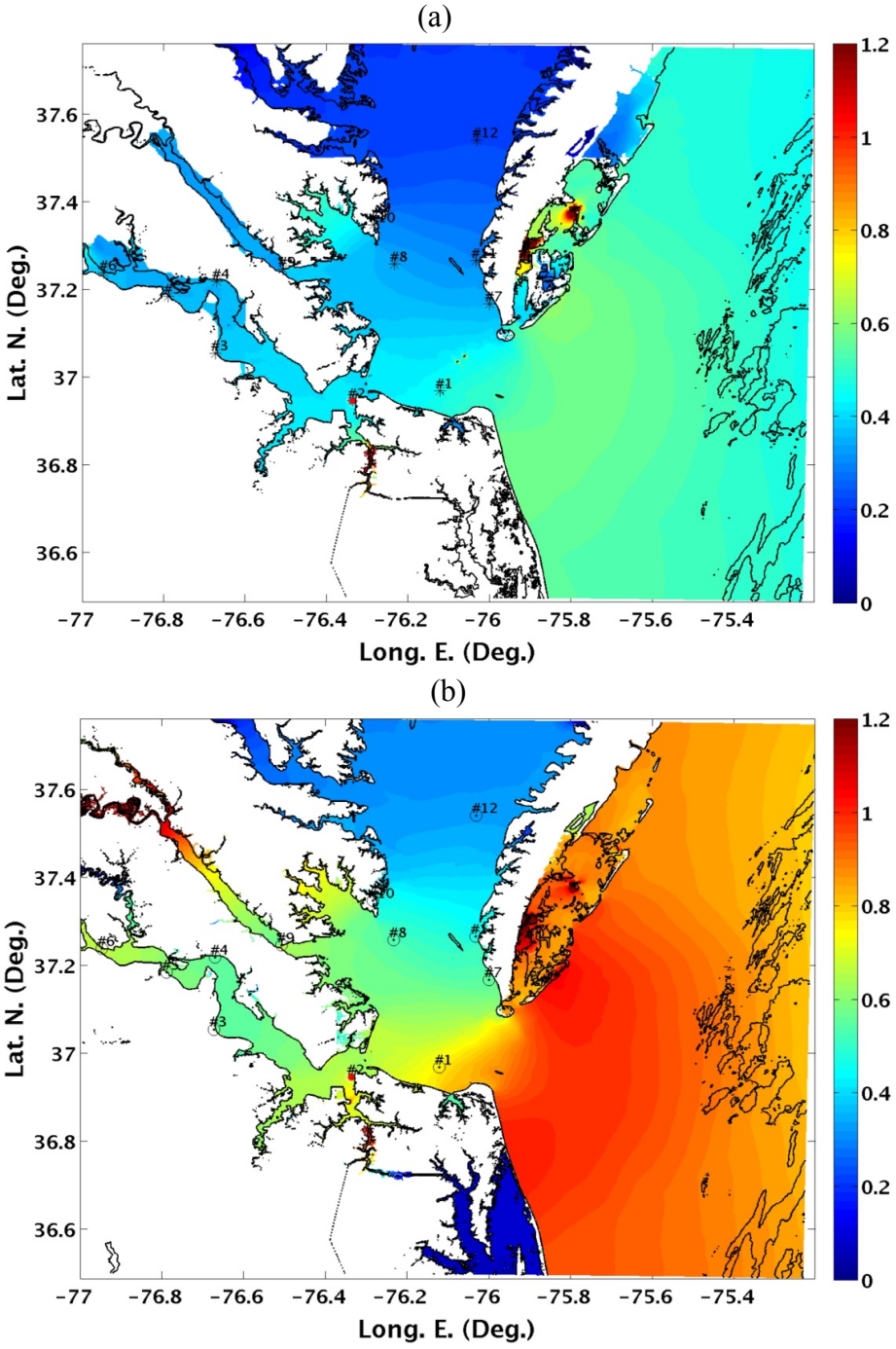

Fig. 12. Envelope of maximum surface elevation (color scale in meter) computed with FUNWAVE-TVD in the 154 m grid (Fig. 2; Table 3), using MHW+SLR as a reference level, for the M2 tide: (a) mean (unscaled) tidal forcing; and (b) scaled tidal forcing (by a 1.9 factor) to achieve AWL (1.244 m NAVD88) at Sewells Point (gage #2), i.e., 10% exceedance tide. Results are for 2.25 tidal periods of simulation (including a quarter period ramp-up). Numbered circles mark locations of 12 NOAA tide gages (Table 5).

Table 5. Results of FUNWAVE-TVD computations for the mean (unscaled) M2 tide, in 154 m grid (Fig. 12a), compared to data at 12 NOAA stations in Chesapeake Bay (Figs. 2 and 3; see http://tidesandcurrents.noaa.gov/stations.html?type=Water+Levels). RMS of relative error on computed range is 8% (based on computed minus reference values).

No.	NOAA Station	Comp. max elevat. (m)	Comp. min elevat. (m)	Comp. range (m)	NOAA range (m)	Relative Error on range (%)	Comp. period (h)	Comp. Phase (from #2) (deg.)	NOAA Phase (from #2) (deg.)
#1	#1:Chesapeake Bay Bridge, VA	0.44	-0.40	0.84	0.76	+9.5	12.50	239.96	220.60
#2	#2: Sewells Point, VA	0.41	-0.37	0.78	0.73	+6.4	12.50	261.70	261.70
#3	#3: Burwell Bay, James River, VA	0.39	-0.24	0.63	0.71	-12.7	12.58	305.18	299.30
#4	#4: Kingsmill, VA	0.37	-0.14	0.51	0.66	-22.7	12.50	343.83	318.00
#5	#5: Scotland, VA	0.35	-0.12	0.47	0.57	-17.8	12.58	360.73	339.20
#6	#6: Tettington, James River, VA	0.37	-0.08	0.45	0.52	-14.4	12.42	46.63	10.60
#7	#7: Kiptopeke, VA	0.37	-0.38	0.75	0.78	-2.9	12.58	244.79	247.50
#8	#8: New Point, VA	0.34	-0.30	0.64	0.62	+3.6	12.50	259.28	256.00
#9	#9: Gloucester Point, VA	0.36	-0.31	0.67	0.72	-7.0	12.67	256.87	268.60
#10	#10: New Point, VA	0.30	-0.20	0.50	0.49	+2.0	12.42	264.12	262.70
#11	#11: Cape Charles Hbr, VA	0.28	-0.30	0.58	0.68	-14.7	12.42	259.28	259.40
#12	#12:Rappahannock Light, VA	0.22	-0.20	0.42	0.48	-11.5	12.50	295.52	301.90

Fig. 14 shows plots of instantaneous tide-induced currents (both magnitude and direction) for the calibrated M2 tide simulation, for 5 stages separated by 3h 6 min (186 min), thus nearly covering one tidal period. Figure 15 shows the corresponding time series of current magnitude at tide stations #1-6. Fig. 14a shows the simulation after 755 s which, based on the time series shown in Figs. 13b and 15, corresponds to a stage where the surface elevation at station #4, upstream the James River, is decreasing and is about 0.16 m below the reference level, and the ebb currents are large (flowing out of the James River), at about 0.5 m/s (1 knot) near station #5 (less at the tide gage station #4, about 0.3 m/s, because it is near the shore). This stage repeats itself in Fig. 14e. Another stage of the simulation with both large currents and elevation near station #4 is shown in Fig. 14c, after 1135 s, for which Figs. 13b and 15 indicate that the surface elevation at station #4 is about 0.53 m and the flooding currents (flowing into the James River) are again large, about 0.5 m/s (about 0.35 m/s at station #4). At other locations in the James River, currents reach up to 0.9 m/s depending on the stage of the tide (locally more).

In the combined tide-tsunami simulations presented next, we will show which stage of the tide (i.e., combination of tidal elevation and current when the main tsunami waves propagate up the river) leads to the worst-case scenario in terms of inundation in the James River.

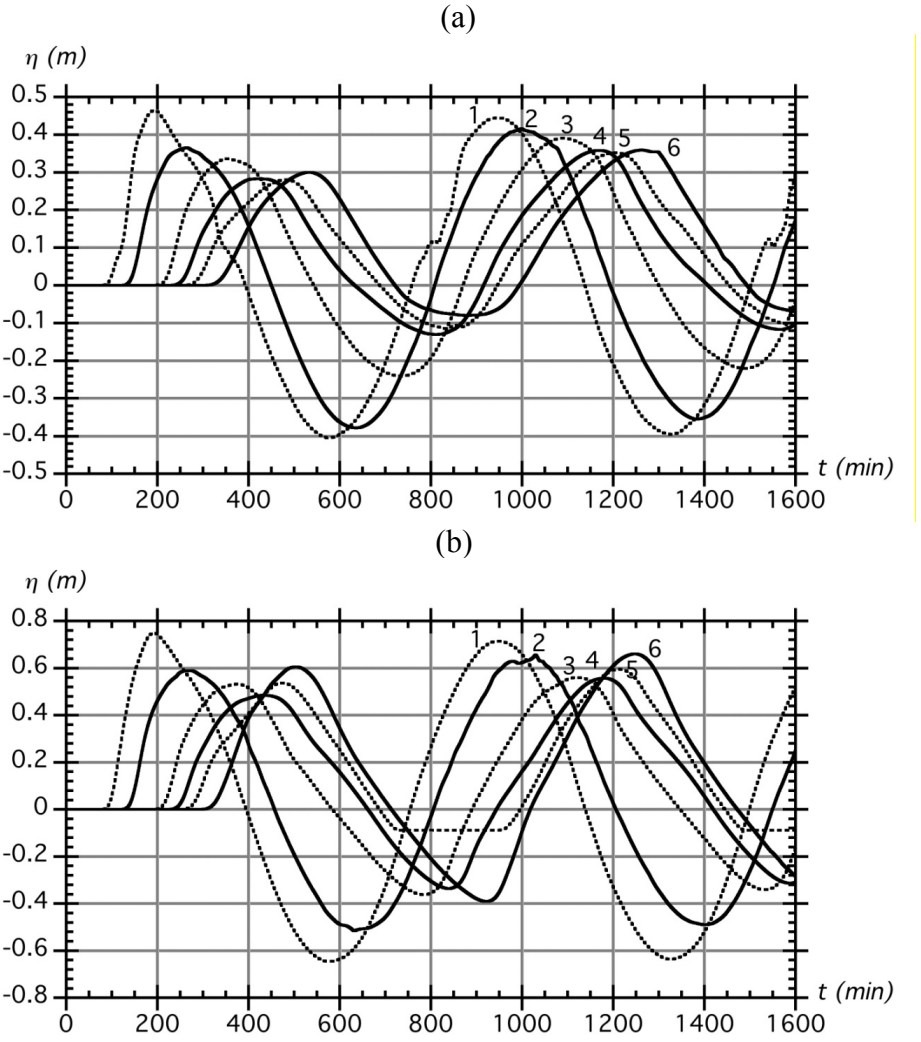

Fig. 13: Time series of surface elevation computed at NOAA stations #1-6 in the James River (Table 5), with FUNWAVE-TVD in the 154 m grid (Fig. 2; Table 3), using MHW+SLR as a reference level, for the M2 tide: (a) mean (unscaled) tidal forcing (case of Fig. 12a); and (b) scaled tidal forcing (by a 1.9 factor; case of Fig. 12b) to achieve AWL (1.244 m NAVD88; 0.957 MHW) at Sewells Point (gage #2), i.e., 10% exceedance tide. Results are for 2.25 tidal periods of simulation (including a quarter period ramp-up).

(a)

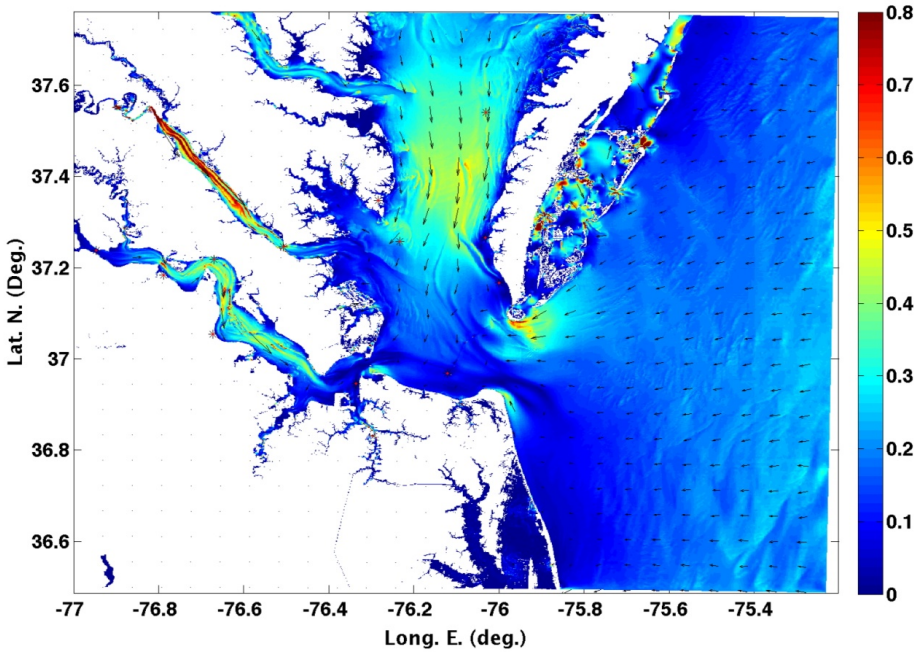
Lat. N. (Deg.)
37.6
37.4
37.2
37
36.8
36.6
-77
-76.8
-76.6
-76.4
-76.2
-76
-75.8
-75.6
-75.4
Long. E. (deg.)
0.8
0.7
0.6
0.5
0.4
0.3
0.2
0.1
0

(b)

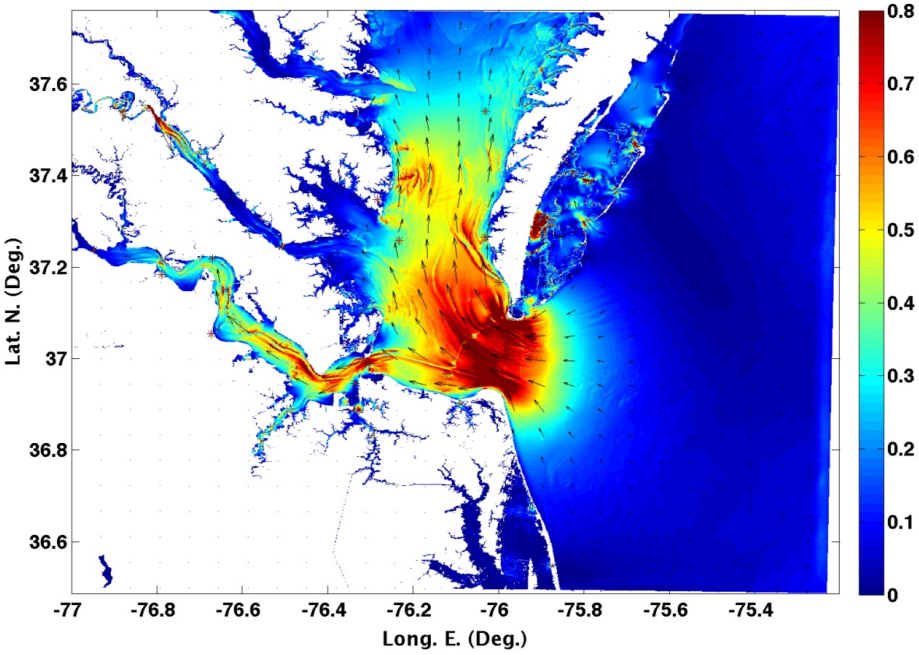
Lat. N. (Deg.)
37.6
37.4
37.2
37
36.8
36.6
-77
-76.8
-76.6
-76.4
-76.2
-76
-75.8
-75.6
-75.4
Long. E. (Deg.)
0.8
0.7
0.6
0.5
0.4
0.3
0.2
0.1
0

(c)

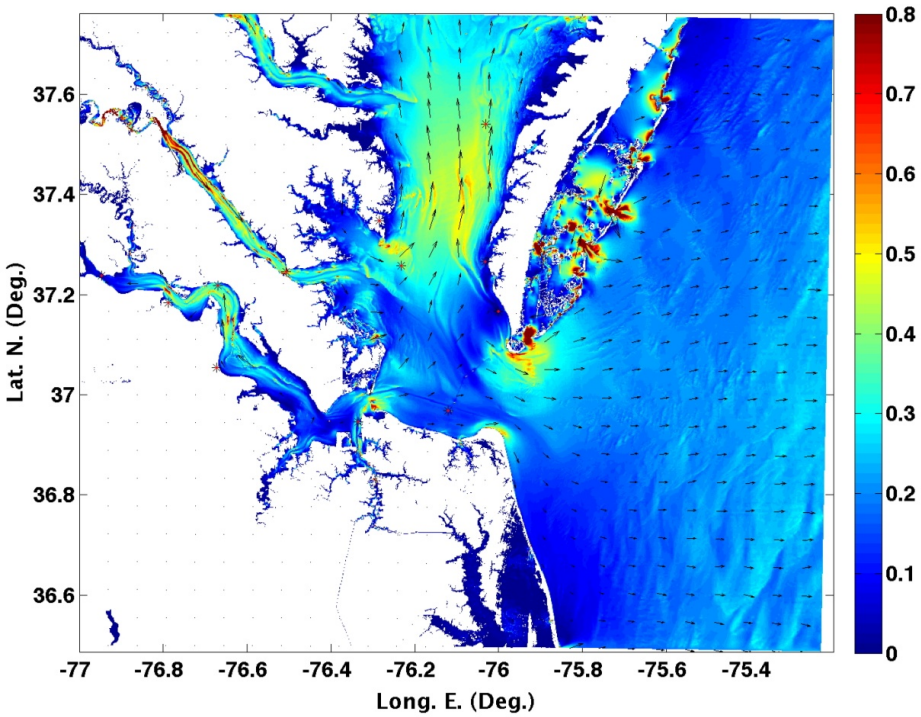
37.6
37.4
37.2
37
36.8
36.6
Lat. N. (Deg.)
-77
-76.8
-76.6
-76.4
-76.2
-76
-75.8
-75.6
-75.4
Long. E. (Deg.)
0.8
0.7
0.6
0.5
0.4
0.3
0.2
0.1
0

(d)

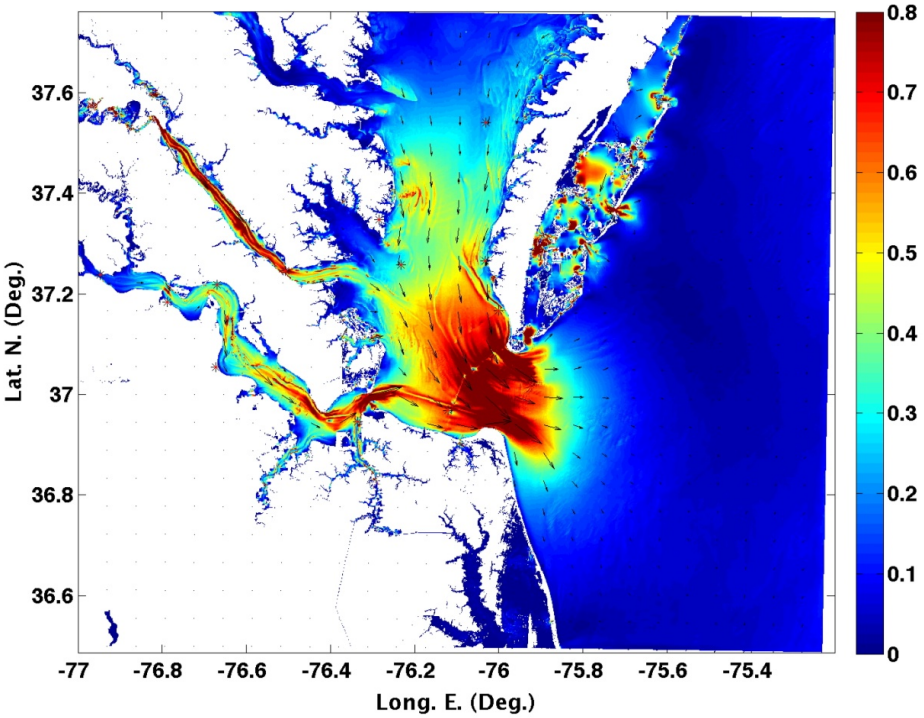
37.6
37.4
37.2
37
36.8
36.6
Lat. N. (Deg.)
-77
-76.8
-76.6
-76.4
-76.2
-76
-75.8
-75.6
-75.4
Long. E. (Deg.)
0.8
0.7
0.6
0.5
0.4
0.3
0.2
0.1
0

(e)

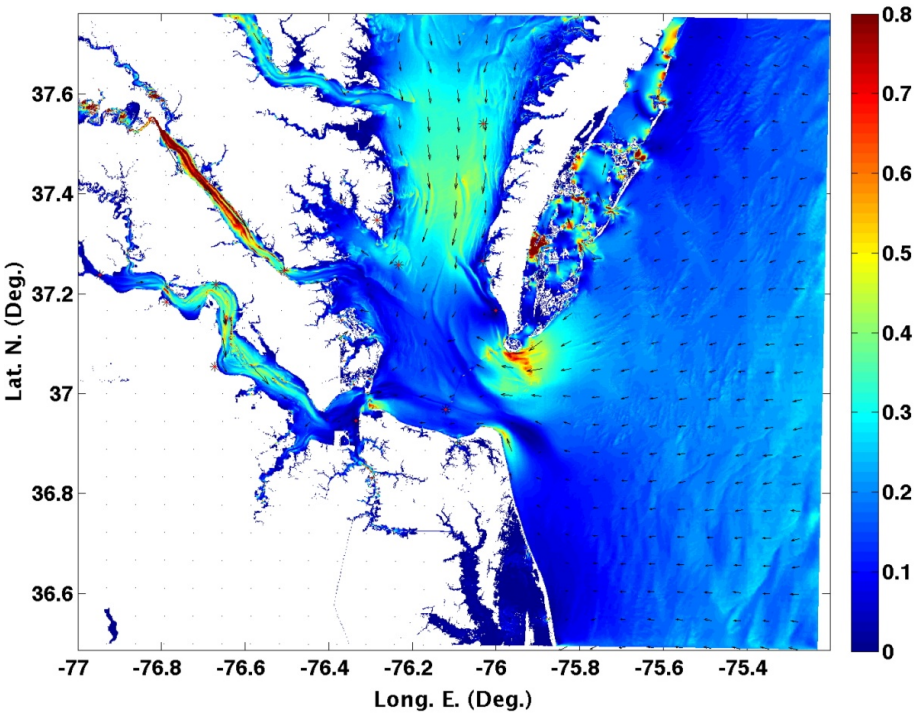

Fig. 14: Instantaneous current magnitude (color scale in m/s) and direction (arrows) computed with FUNWAVE-TVD in the 154 m grid (Fig. 2; Table 3), using MHW+SLR as a reference level, for the scaled M2 tide (by a 1.9 factor; case of Fig. 12b). Results are at *t* = (a) 755; (b) 945; (c) 1135; (d) 1325; and (e) 1515 min. into the simulation (186 min. intervals, about a quarter period). Red stars mark locations of NOAA tide gage stations (see Table 5).

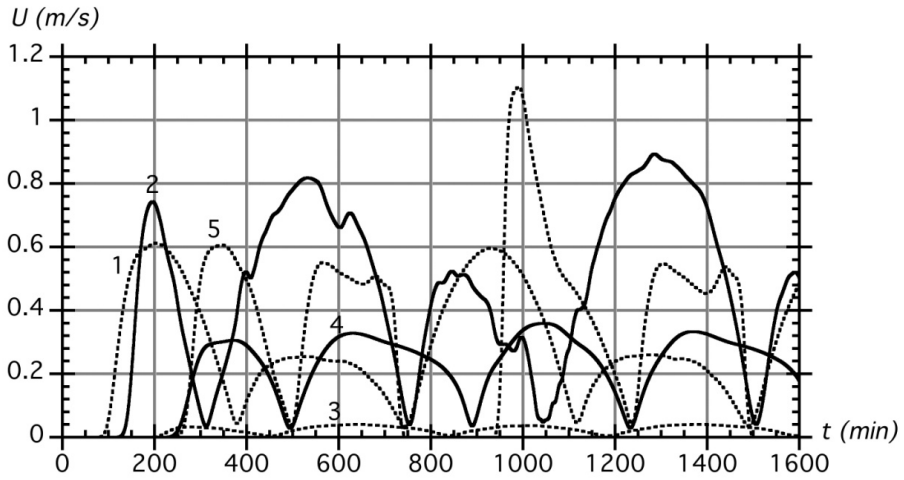

Fig. 15: Time series of current magnitude at NOAA stations #1-5 in the James River (Table 5), computed with FUNWAVE-TVD in the 154 m grid (Fig. 2; Table 3), using MHW+SLR as a reference level, for the scaled M2 tide (by a 1.9 factor; case of Fig. 12b).

5. Modeling tide-tsunami interactions

We perform combined simulations with FUNWAVE-TVD of tide and tsunami interactions by superimposing time series of incident CRT and CVV wave trains and the calibrated (scaled up) M2 tide that creates AWL conditions for the MHW+SLR reference level, along the boundary of the 154 m grid. Simulations are performed in this grid and continued by one-way coupling in the finer nested 39 m grid (Fig. 3), in order to more accurately resolve tsunami inundation in the James River and study tide-tsunami interactions.

Because both tide and tsunami are long waves, they are expected to propagate at the same phase speed in the shallow waters of the Chesapeake Bay and the shelf off of it. Hence, to the first-order (i.e., neglecting nonlinear effects) if one superimposes a phase of the tide with the maximum elevation in the tsunami train (here the first crest) along the offshore boundary of the 154 m grid, then one should expect those "phases" to propagate together, including up the James River. Nonlinearity, however, will affect this superposition and both create time lags between tide and tsunami maxima and spreading out of the tsunami wave train, particularly when the current (of either the tide, the tsunami or both) is large.

The first tidal phase (referred to as TT1) we consider is when both tide and maximum tsunami waves are synchronized on the offshore boundary, thus causing maximum elevation in the James River by way of superposition. The second situation (referred to as TT2) is selected when the tide level is starting to decrease from its maximum, by specifying the maximum tsunami at about one-eighth tidal period after the maximum tide. The third phase (referred to as TT3) is selected when the ebb current is quite large in the river (e.g., Fig. 14d), thus flowing against the incoming tsunami and possibly causing it to shoal up; this is achieved by specifying the maximum tsunami when the tide is crossing the zero level going down, at one-fourth tidal period after the maximum tide. Finally, a last phase (referred to as TT4) is selected at one-eight tidal period ahead of the maximum tide, thus superposing the maximum tsunami with a rising tide.

Full details of results will be provided for the TT1 case, for both the CVV and CRT tsunamis. Then, we will show comparisons of selected results obtained for the four phases of the tide, in order to assess which tide-tsunami interaction processes lead to increased inundation in the river.

5.1 Joint simulations of maximum tide and tsunami (TT1)

Far-field subaerial landslide (CVV). Fig. 16a shows the surface elevation from the superposition of the incident CVV tsunami wave train with the calibrated M2 tide elevation at the SE corner of the 154 m grid, for the TT1 phase situation; as expected, the maximum tsunami and tide elevations have been synchronized. The computed time series of surface elevation at the Sewells Pt. reference station (NOAA tide gauge #2; Table 5), plotted on the same figure, shows a strong reduction of the CVV tsunami elevation across the wide shelf and in the shallow entrance of the Chesapeake Bay, due to both directional spreading and dissipation of the larger incident waves mostly by bottom friction (and some breaking). From a maximum elevation of 8 m on the

offshore boundary of the 154 m grid, the tsunami elevation at Sewells Pt. is reduced to 1.7 m. Many of the smaller oscillations in the incident wavetrain have disappeared, being damped out.

Computations are pursued by one-way coupling in the 39 m grid. Fig. 16b first shows that there is a good agreement of the tsunami surface elevation computed at Sewells Pt. in both grids, with expectedly more higher frequency oscillations occurring in the 39 m grid, owing to the better resolution.

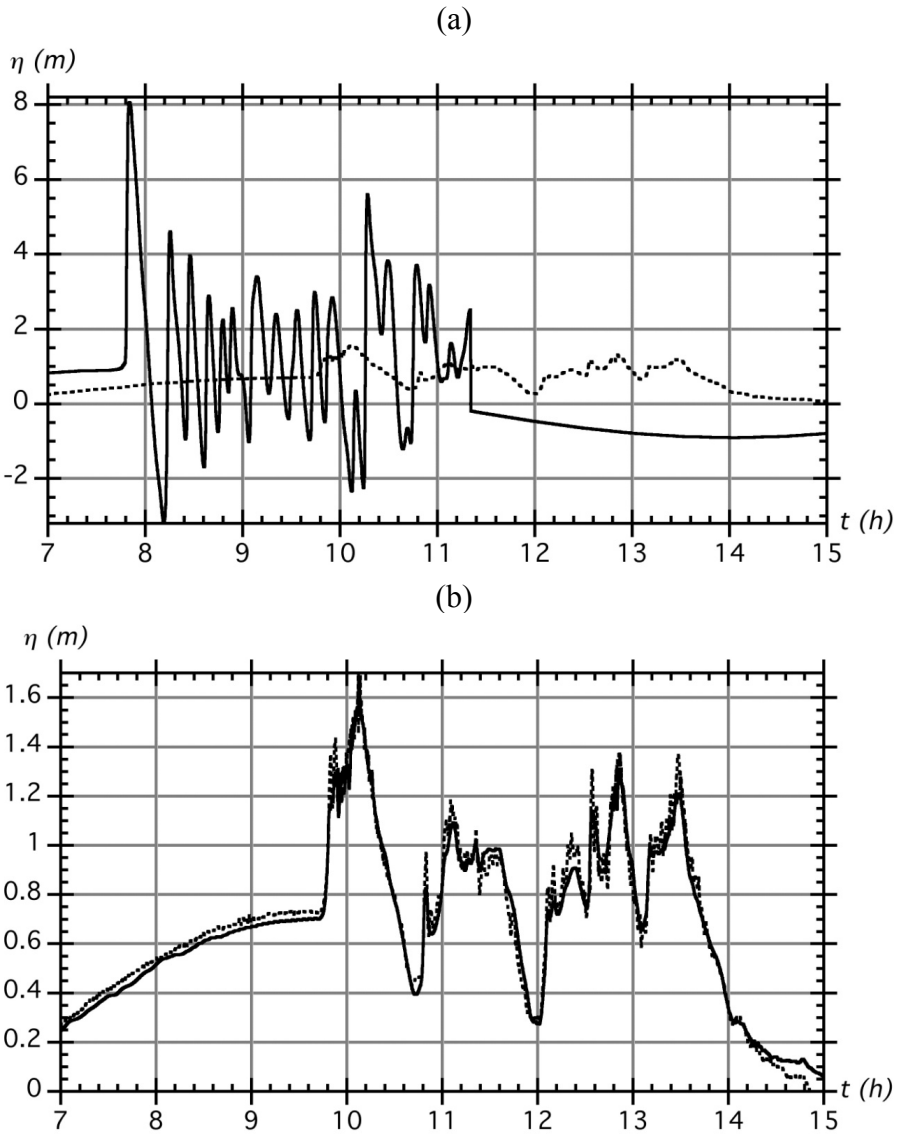

Fig. 16: Simulation with FUNWAVE-TVD (MHW+SLR reference level) of the calibrated M2 tide plus CVV tsunami (TT1 phase situation). Time series of surface elevation at: (a) SE corner (solid) and NOAA station #2 Sewells Pt (dashed), in 154 m grid (Fig. 2); (b) at NOAA station #2 Sewells Pt, in 154 m grid (solid) and in 39 m grid (Fig. 3) (dashed). Time is from the start of the CVV event

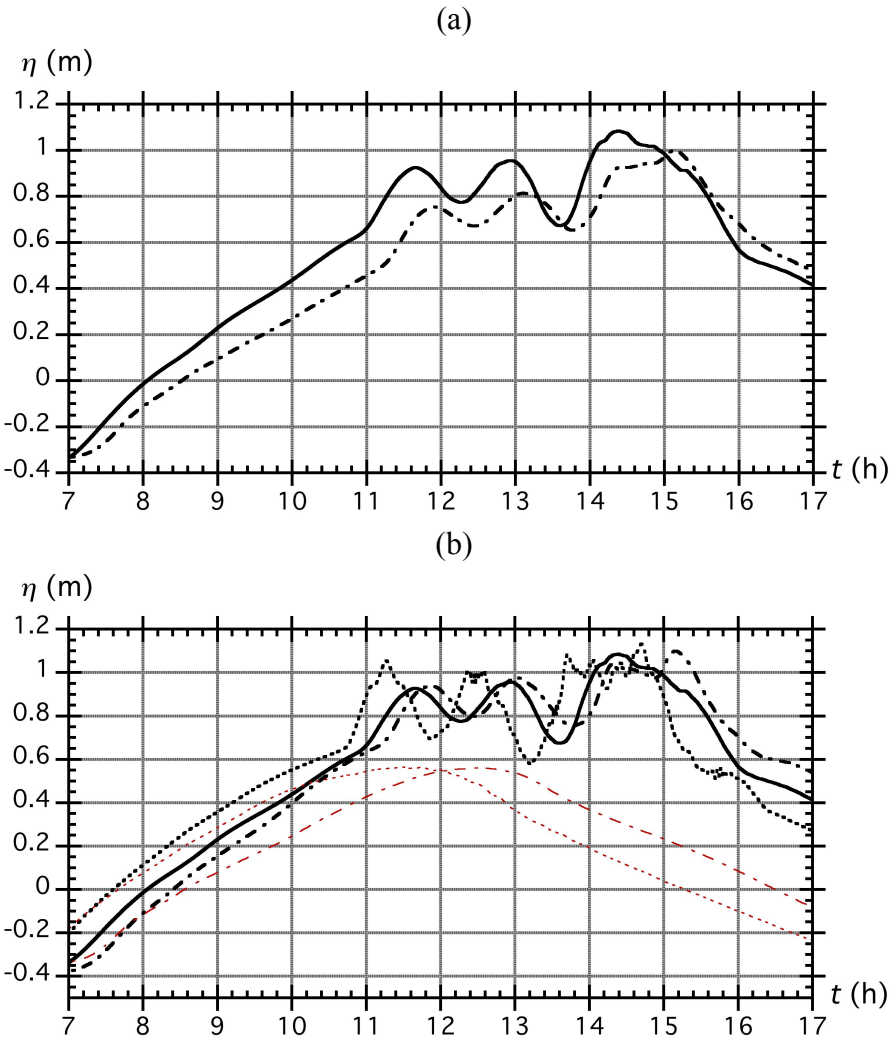

Fig. 17: Simulation with FUNWAVE-TVD (MHW+SLR reference level) of the calibrated M2 tide plus CVV tsunami (TT1 phase situation). Time series of surface elevation at: (a) "river station" (Fig. 3), in 154 m (chained) and 39 m grids (solid); (b) Station #3 (thick dashed), Station #4 (thick chained) and the "river station" (thick solid) in 39 m grid. Thin red lines in (b) show the tide only results at Stations #3 and #4. Time is from the start of the CVV event.

Fig. 17a then compares the surface elevations computed at the so-called "river station" (Fig. 3), located upstream and in the middle of the James River (-76.64 E, 37.15 N), in the 154 m and 39 m grids. The agreement is good, but elevations in the finer grid are up to 0.15 m higher than in the coarser grid, which justifies using the 39 m grid to compute tsunami inundation levels in the James River. Compared to Fig. 16 at Station #2, we also see that during its propagation up the James River, the tsunami wave train has lost all of its higher-frequency oscillations and is reduced to three main oscillations of about 1.5 hour period; also, unlike in Fig. 16, the larger elevations occur later in the wave train. Fig. 17b then shows results computed in the 39 m grid at NOAA Stations #3 and #4, with the "river station" used as a reference (Fig. 3), compared to surface elevations obtained for the calibrated M2 tide only. As expected for TT1, the leading

tsunami and tide elevations are almost synchronized. However, higher surface elevations are seen to occur for later times in the wave train, likely due to an enhancement of smaller incident tsunami waves by the ebbing tidal currents.

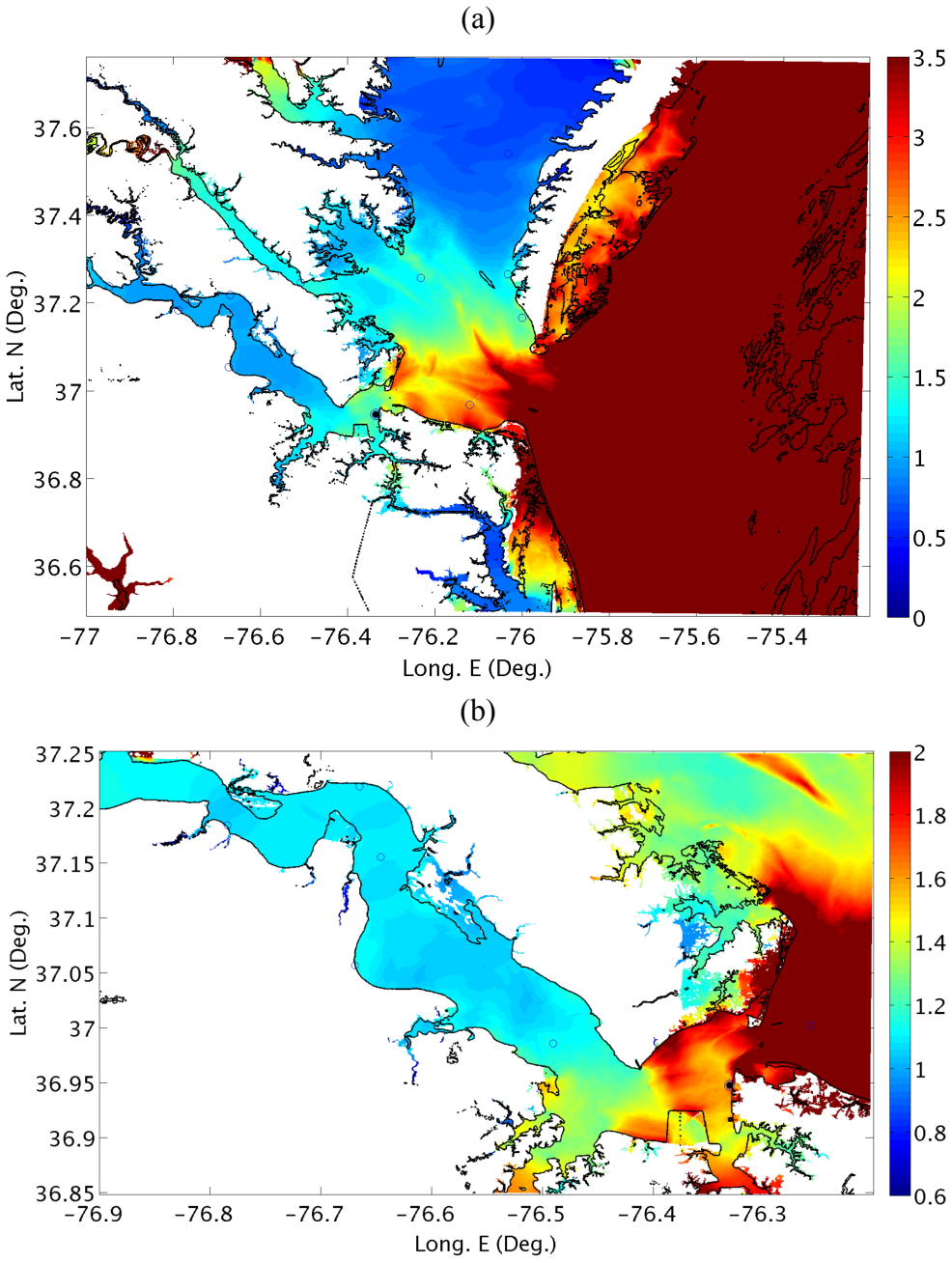

Fig. 18: Simulation with FUNWAVE-TVD (MHW+SLR reference level) of the calibrated M2 tide plus CVV tsunami (TT1 phase situation). Envelope of maximum surface elevation in: (a) 154 m grid; (b) 39 m grid. Circles mark locations of the NOAA stations (Table 5) and the "river station"; solid circle symbol is Sewells Point (Station #2).

Finally, Fig. 18 shows the envelope of maximum surface elevation computed for this case in both the 154 m and 39 m grids. While at and near the James River mouth, maximum tsunami inundation reaches 2-2.5 m, in the river, we see a significant decrease in maximum inundation, in the 1.1-1.5 m range. Nevertheless, Fig. 18b shows that many low lying areas of the river banks would be flooded.

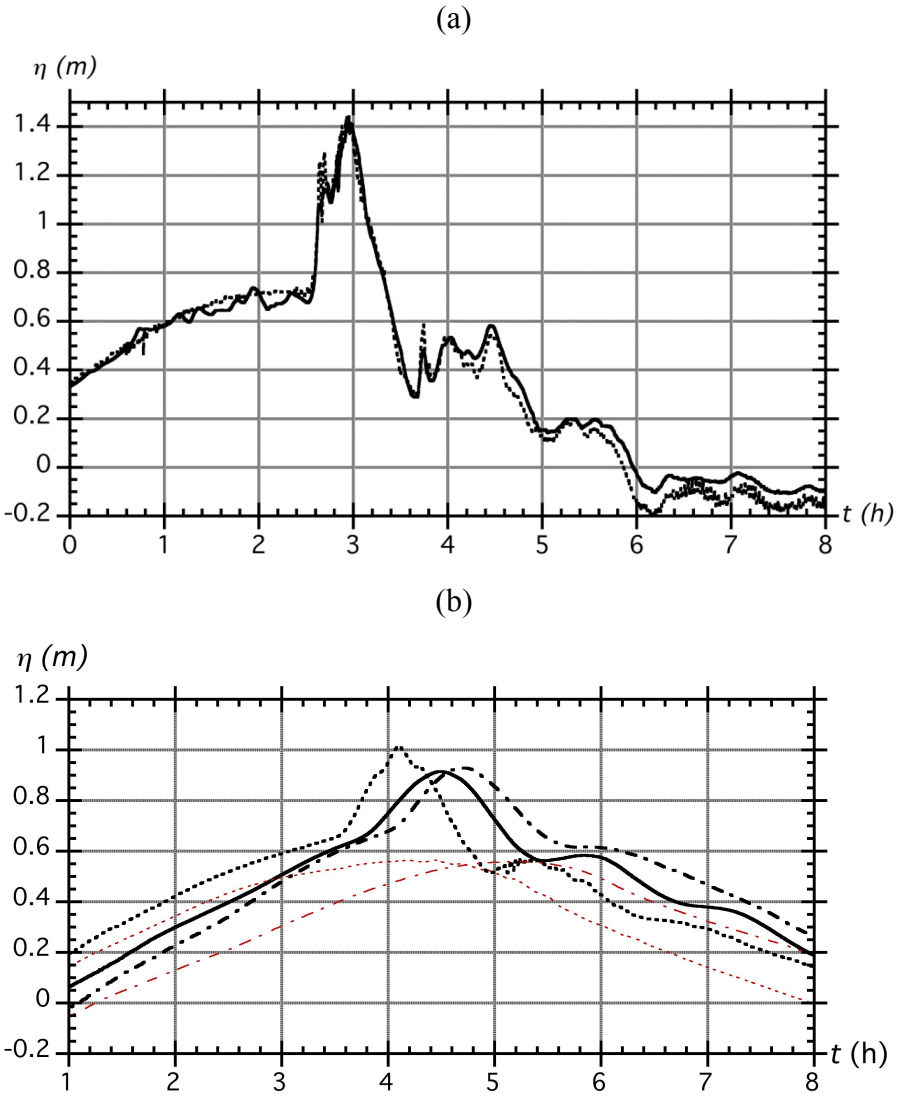

Fig. 19: Simulation with FUNWAVE-TVD (MHW+SLR reference level) of the calibrated M2 tide plus CRT tsunami (TT1 phase situation). Time series of surface elevation at: (a) Sewells Point (Fig. 3), in 154 m (solid) and 39 m grids (dashed); (b) Station #3 (thick dashed), Station #4 (thick chained) and the "river station" (thick solid) in 39 m grid. Thin red lines in (b) show the tide only results at Stations #3 and #4. Time is from the start of the CRT event.

Near-field Submarine Mass Failure (CRT). Fig. 19a shows computed time series at Sewells Point (NOAA station #2; Table 5) of the CRT tsunami elevation combined with the calibrated M2 tide, in both the 154 m and 39 m grids. As expected, the maximum tsunami and tide elevations have been synchronized. Comparing to the large incident tsunami elevation (without

tide) at the offshore boundary of the 154 m grid shown in Fig. 7, similar to the CVV case, there has been a strong reduction of the tsunami elevation across the wide shelf and the shallow entrance of the Bay, due to both directional spreading and dissipation of the large incident waves by bottom friction and some breaking. From a maximum elevation of 4-9 m along the offshore boundary of the 154 m grid, the tsunami elevation at Sewells Point is reduced to 1.45 m.

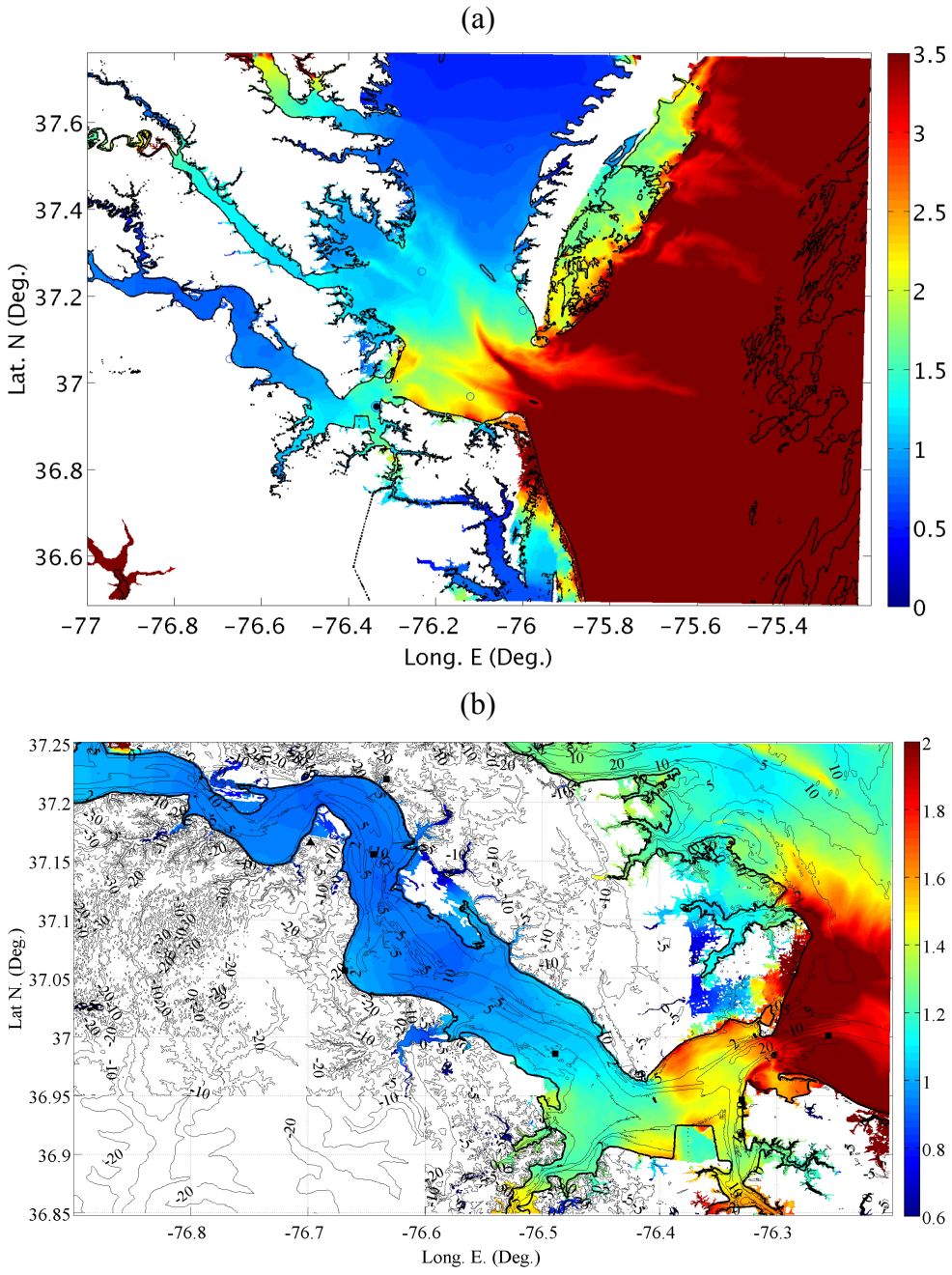

Fig. 20: Simulation with FUNWAVE-TVD (MHW+SLR reference level) of the calibrated M2 tide plus CRT tsunami (TT1 phase situation). Envelope of maximum surface elevation in: (a) 154 m grid; (b) 39 m grid. Circles/black squares mark locations of the NOAA stations (Table 5) and the "river station"; solid circle symbol is Sewells Point (Station #2).

Similar to the CVV case, Fig. 19b shows results computed in the 39 m grid at NOAA Stations #3 and #4, with the "river station" used as a reference (Fig. 3), compared to surface elevations obtained for the calibrated M2 tide only. The leading tsunami and tide elevations are again almost synchronized but this time the highest combined surface elevations occur for the leading crest in the wave train, with about 0.9-1 m above the MHW+SLR reference level. Compared to Fig. 19a at Station #2, we again see that during its propagation up the James River, the tsunami wave train has lost all of its higher-frequency oscillations and as for CVV is reduced to three main oscillations of about 1.5 hour period

Finally, Figure 20 shows the envelope of maximum surface elevation computed for this case in both the 154 m and 39 m grids. While at and near the James River mouth, maximum tsunami inundation reaches 1.5-2 m, in the river, however, we see a significant decrease in maximum inundation, in the 0.9-1.1 m range. Although less than for CVV, Fig. 20b shows that some low lying areas of the river banks would be flooded for this case as well.

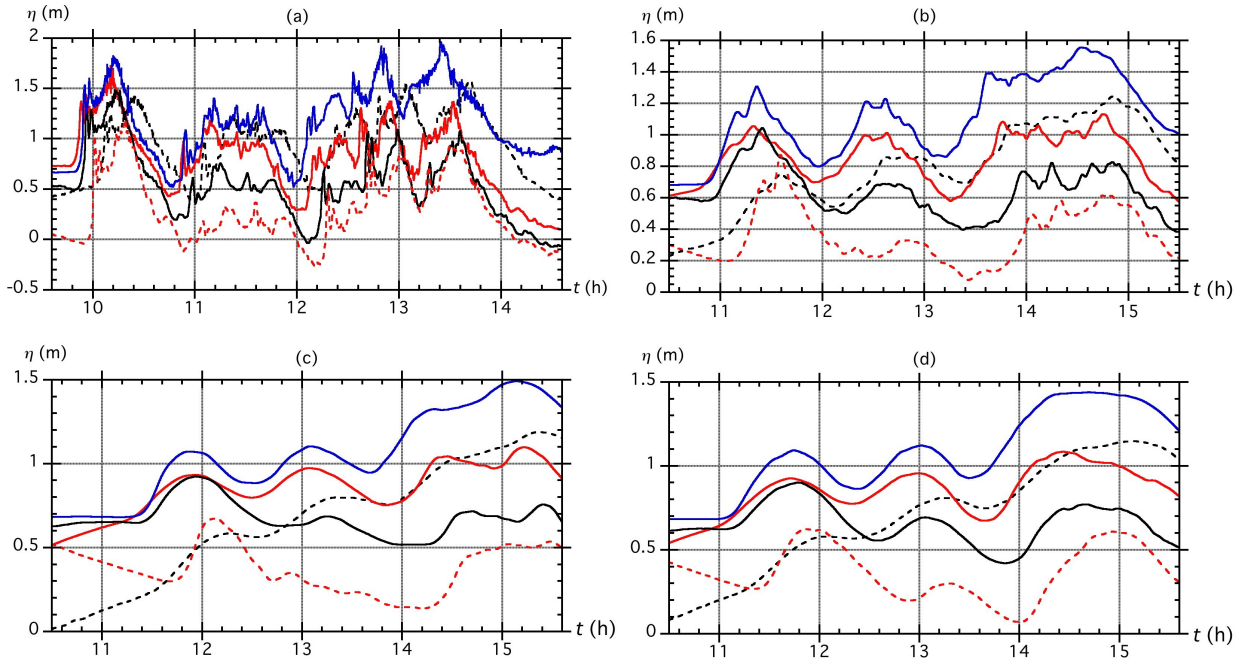

Fig. 21: Simulation with FUNWAVE-TVD (MHW+ SLR reference level) of the CVV tsunami plus the calibrated M2 tide for phase: TT1 (solid red); TT2 (solid black); TT3 (dashed red); and TT4 (dashed black). Time series of surface elevation at station (Fig. 3; Table 5): (a) #2 (Sewells Point); (b) #3 (c) #4 and (d) "river station". For comparison, we plotted with reference to MHW+SLR (solid blue) the CVV tsunami computed on a static reference level AWL (0.957 m MHW) (CVVSL). Time is shown from the start of the CVV event.

5.2 Joint simulations of tide and tsunami for other phases of the tide

Far-field subaerial landslide (CVV).

Figure 21 shows computed surface elevations in the 39 m grid, at 4 gauges (Fig. 3; Table 5): #2 (Sewells Pt), #3, #4 and the "river station", for the superposition of the incident CVV tsunami

with the calibrated M2 tide, for the 4 phases of the tide (with respect to the MHW + SLR reference level). Additionally, for comparison, we plotted results of computations of the CVV tsunami over a reference static level equal to the AWL (0.957 m MHW), with respect to the same reference level (MHW + SLR); this is referred to as CVVSL in the following.

In all cases, we see a gradual reduction of the maximum surface elevation when moving up the James River, from Sewells Pt. to station #4, due to bottom friction in the gradually shallower river and its banks. For the cases TT2 and TT3 the first two tsunami wave crests are seen to reach all the stations at almost the same time as for the CVVSL case. Likely due to the ebb current effects, for phases TT1 and TT4, however, we see that the arrival of the tsunami wave crests is gradually more delayed, when moving upstream. Regarding maximum water level, while the first crest for case TT1 reaches nearly the same level as the CVVSL case, later on and up the river, as the tide level both decreases due to bottom friction and to the tidal variation in time, the maximum water level for any phase case is never higher than that calculated for CVVSL; hence, this approach which is recommended by NRC for tsunami hazard assessment appears to be conservative in the present case, despite the presence of tidal currents. However, comparing among computations for the various tide phases, we see that the case TT4, which starts at a lower level than all the other cases but TT3 at Sewells Pt, ends up causing higher surface elevations at all stations upstream the river, although it takes a few hours for this to occur. This is clearly a result of dynamic effects of tide and tsunamis current interactions (this will be further analyzed later). The next higher level is achieved for the case TT1 and then cases TT2 and TT3 are always lower than the other cases. Finally, depending on the case, when tide and tsunami interact, other waves in the wave train can end up being amplified, thus causing larger flooding; for instance, the third crest is that with the highest amplitude in the TT4 phase.

To more clearly assess tide and tsunami interactions, Figs. 22 and 23 show the computed current magnitude (m/s) and direction at the Sewells station #2 and at station #4, upstream the James River (Fig. 3; Table 5), for the CVV tsunami alone (CVVSL case), the calibrated M2 tide alone, and the TT1 and TT4 phase combinations, which were seen to cause the worst case scenarios as far as surface elevation. As expected from the water level results, current velocities for the combined tsunami-tide cases are always larger at Sewells Pt than those at station #4, with maximum values 0.55 m/s and 0.42 m/s for case TT4, respectively; when propagating upstream, the current speed decreases and higher frequency fluctuations are gradually damped out as a result of bottom friction, similar to what was observed for surface elevations. Although the maximum velocity is slightly larger at Sewells Pt for the tsunami alone case (0.6 m/s in its tail), than when combined with the tide for TT1 or TT4 phases, it is larger at station #4 when combined with the tide, for the two latter cases, than for the tsunami or tide alone cases; this results from destructive or constructive interferences with the tide, respectively. Finally, it can be seen that because of interactions with tidal currents, the direction of currents in the TT1 and TT4 case is different from the CVVSL case at various times of propagation at both stations. This clearly illustrates the site and case specific nature of tsunami-tide interactions, and that these

cannot be anticipated by simple linear superposition, as there are strong nonlinear effects when combining tsunami and tidal currents (such as related to bottom friction).

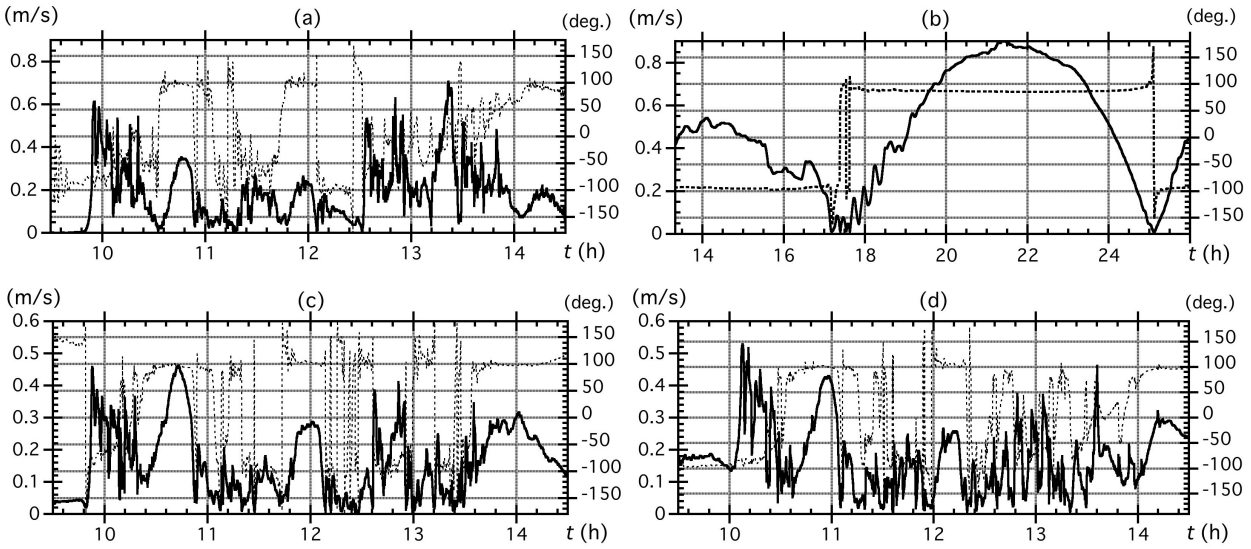

Fig. 22: Simulation with FUNWAVE-TVD (MHW+ SLR reference level) of the CVV tsunami and calibrated M2 tide. Time series of current magnitude (solid) and direction (dashed; in degree with respect to east) at Sewells Pt station #2 (Fig. 3; Table 5): (a) tsunami alone; (b) tide alone; tsunami plus tide for phase (c) TT1, and (d) TT4. Tsunami and TT1/TT4 simulations are in 39 m grid, and time shown is from the start of the CVV event. Tide alone simulations are in 154 m grid, and time shown is total time of tide simulation, starting at 13.33 h (800 s) when the second tidal cycle is zero-up-crossing at Sewells Pt. (curve 2 in Fig. 13b).

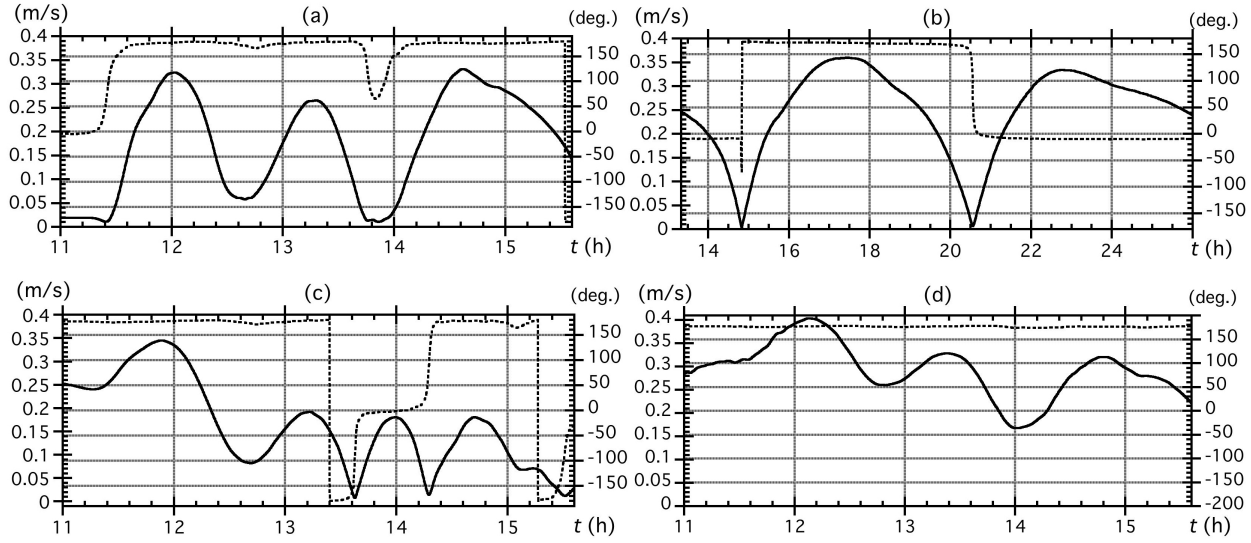

Fig. 23: Same case as in Fig. 22 for results at Station #4 in the James River (Fig. 3; Table 5).

To provide a comprehensive picture of maximum tsunami inundation, Fig. 24 shows the envelope of maximum surface elevation computed for the CVV event in the 39 m grid, for the different phases TT1 to TT4. Again, we see the strong reduction of surface elevation observed for all phases in Fig. 21 when moving upstream. From a maximum elevation of over 2 m at the mouth of the James River, the maximum elevation is reduced to about 1.0-1.1 m up the river.

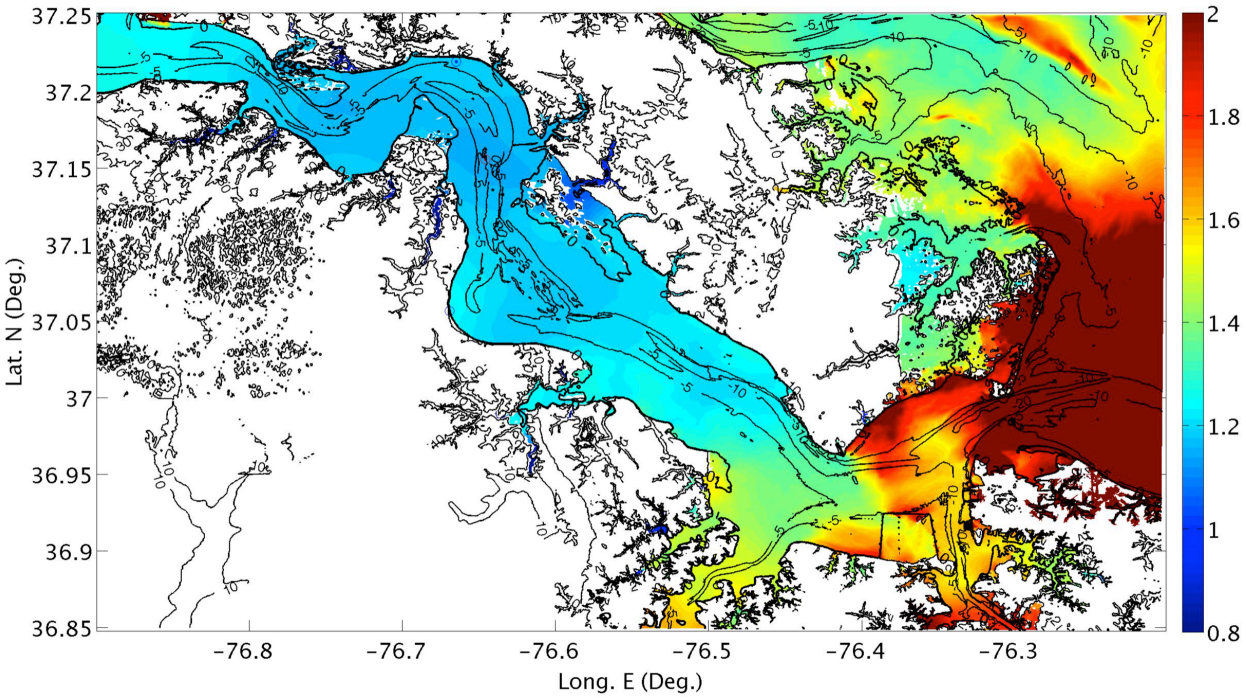

Fig. 24: Simulation with FUNWAVE-TVD (MHW+SLR reference level) of the calibrated M2 tide plus CVV tsunami. Envelope of maximum surface elevation (colorbar in meter) computed in 39 m grid for all tide phases (TT1, TT2, TT3 and TT4).

Near-field Submarine Mass Failure (CRT).

The same comparison as for CVV, among simulation results obtained for various tide phases, is repeated for the CRT tsunami. In Fig. 25 we see this comparison for surface elevations; although the incident tsunami wave train is quite different from that of CVV, we observe the same overall behavior, with a gradual decrease in maximum surface elevation when moving upstream the James River, and the case TT4 being again the worst-case scenario in terms of maximum inundation level. In fact, at Sewells Pt, although initially cases TT1 and CRTSL cause a higher surface elevation, later on case TT4 causes a larger inundation than the TT1 case, and for quite a long time. However, as far as maximum level reached at any gauge, CRTSL still is higher than results from the dynamic tide-tsunami simulations and, hence, the static approach, although quite artificial for a tide-driven flow in an estuary, can still be deemed to be conservative in the present case. Among the various tide phases, unlike for CVV, here, TT1 provides the worst case scenario

in terms of maximum level reached at any gage. As the tsunami wave train of CRT has just one main peak, the interaction of this maximum crest when synchronized with the maximum tide (i.e., case TT1) generates the maximum flooding effect, and the ebb and flood currents have a smaller impact here in amplifying the tail of the wave train. Also, when moving upstream, and even more so than for CVV, we see a gradual smoothing out of tsunami waves, with first the damping out of higher frequency oscillations and then a gradual flattening of even the longer waves in the incident tsunami wave train. As this process is much stronger for the tide phases, particularly for TT2 and TT3, than for the static CRTSL case, this is clearly another effect of tsunami tide current interactions (this aspect again is analyzed in more details later). Finally, there is a stronger time lag of the arrival of the tsunami wave crests at the various gauges, when combined with the tide, with respect to the static CRTSL case than for the CVV tsunami.

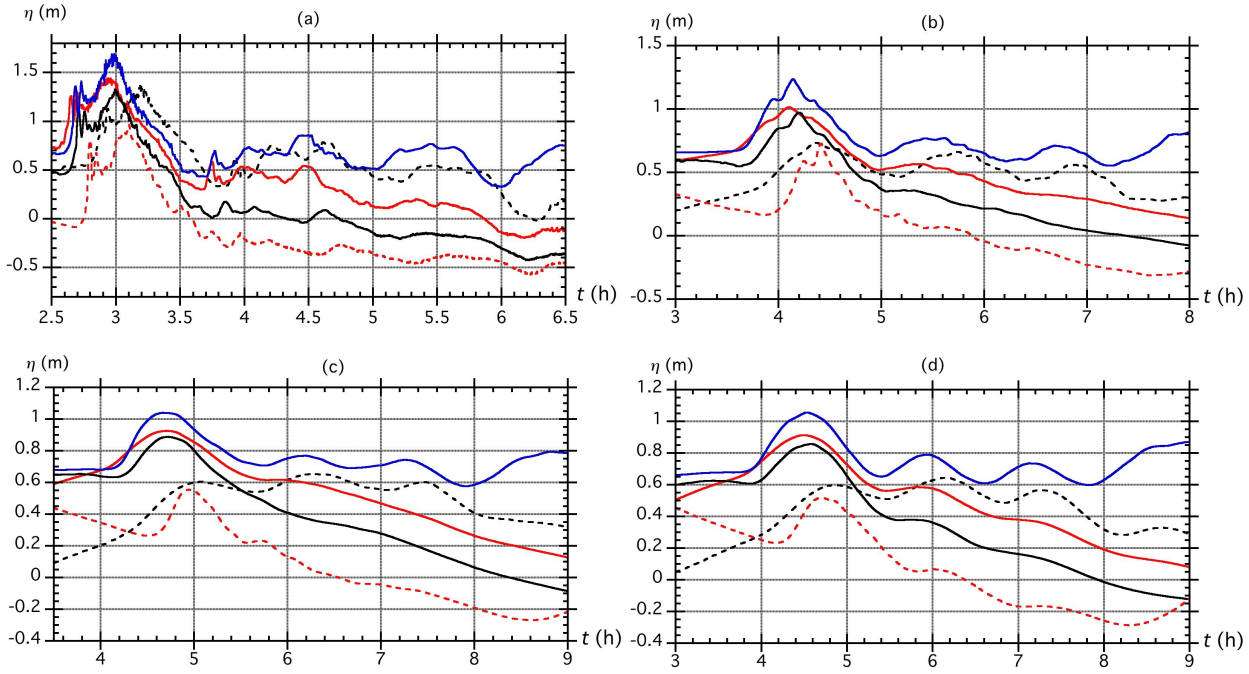

Fig. 25: Simulation with FUNWAVE-TVD (MHW+ SLR reference level) of the CRT tsunami plus the calibrated M2 tide for phase: TT1 (solid red); TT2 (solid black); TT3 (dashed red); and TT4 (dashed black). Time series of surface elevation at station (Fig. 3; Table 5): (a) #2 (Sewells Point); (b) #3 (c) #4 and (d) "river station". For comparison, we plotted with reference to MHW+SLR (solid blue) the CVV tsunami computed on a static reference level AWL (0.957 m MHW) (CRTSL). Time is shown from the start of the CRT event.

Similar to the CVV case, Figs. 26 and 27 show the computed current magnitude (m/s) and direction at the Sewells station #2 and at station #4 (Fig. 3; Table 5), respectively, for the CRT tsunami alone (CRTSL case), the calibrated M2 tide alone, and the TT1 and TT4 phase combinations, which were seen to again cause the worst case scenarios as far as surface elevation. As expected from the water level results, current velocities for the combined tsunami-tide cases are always larger at Sewells Pt than those at station #4, with maximum values 0.48 m/s and 0.37 m/s for case TT4, respectively; similar to CVV, when propagating upstream, the current

speed decreases and higher frequency fluctuations are gradually damped out as a result of bottom friction, similar to what was observed for surface elevations.

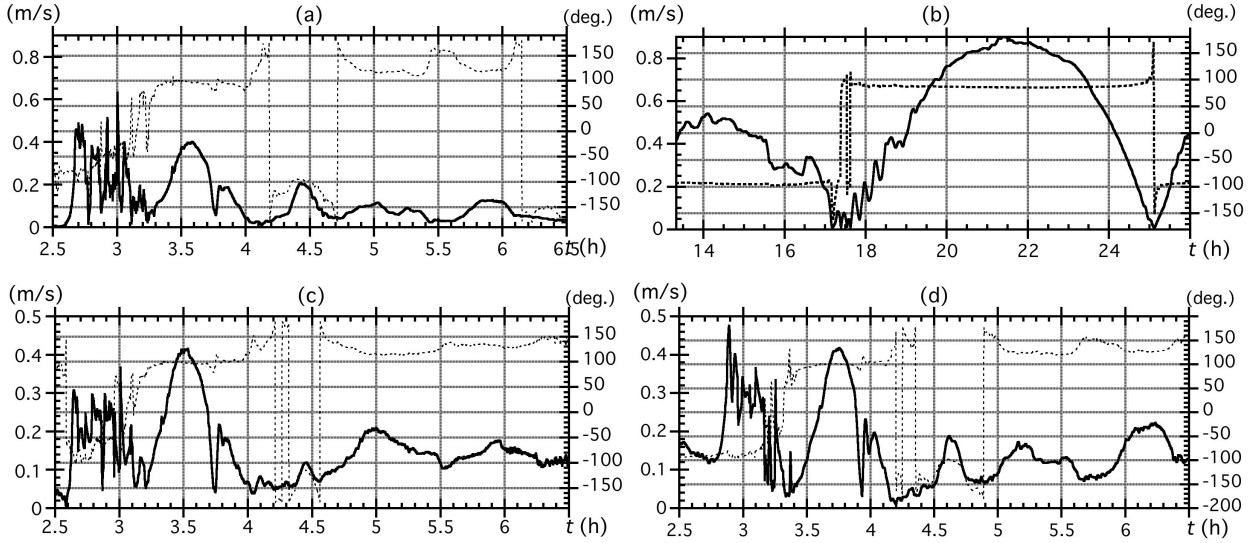

Fig. 26: Simulation with FUNWAVE-TVD (MHW+ SLR reference level) of the CRT tsunami and calibrated M2 tide. Time series of current magnitude (solid) and direction (dashed; in degree with respect to east) at Sewells Pt station #2 (Fig. 2; Table 5): (a) tsunami alone; (b) tide alone; tsunami plus tide for phase (c) TT1, and (d) TT4. Tsunami and TT1/TT4 simulations are in 38 m grid, and time shown is from the start of the CRT event. Tide alone simulations are in 154 m grid, and time shown is total time of tide simulation, starting at 13.33 h (800 s) when the second tidal cycle is zero-up-crossing at Sewells Pt. (curve 2 in Fig. 13b).

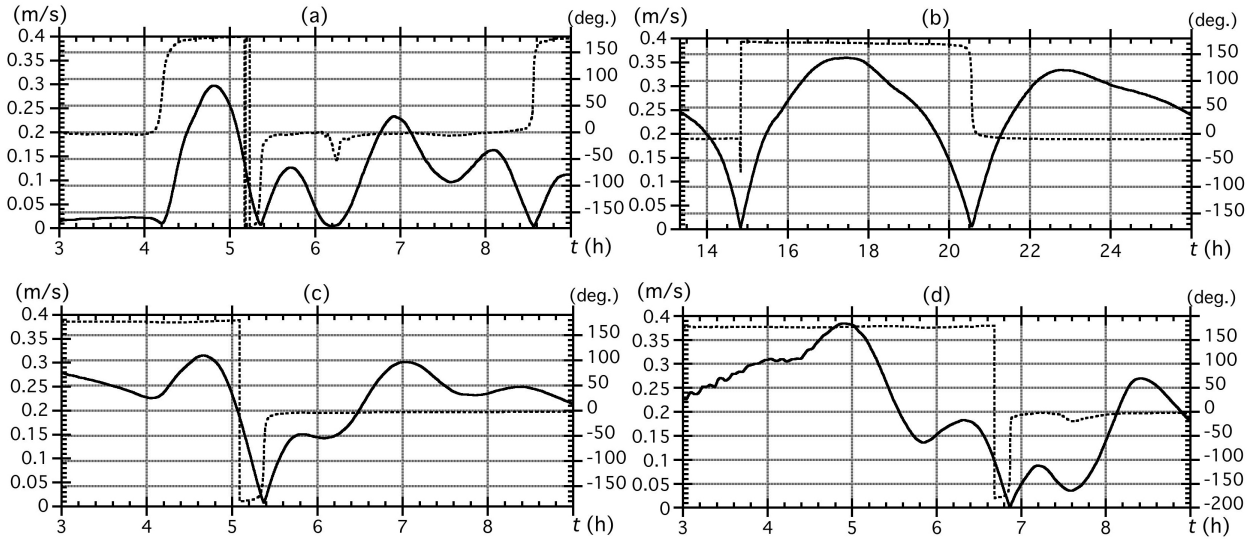

Fig. 27: Same case as in Fig. 26 for results at Station #4 in the James River (Fig. 2; Table 5).

Although the maximum velocity is slightly larger at Sewells Pt for the tsunami alone case (0.65 m/s), than when combined with the tide for TT1 or TT4 phases, it is larger at station #4 when combined with the tide, for the two latter cases, than for the tsunami or tide alone cases. Finally, it can be seen that because of interactions with tidal currents, the direction of currents in the TT1 and TT4 case is different from the CTRSL case at various times of propagation at both stations. This confirms the importance of doing case and site specific studies of tide and tsunami interactions in the presence of strong tidal currents.

To provide a comprehensive picture of maximum tsunami inundation, Fig. 28 shows the envelope of maximum surface elevation computed for the CRT event computed in the 39 m grid for the different phases TT1 to TT4. We again see the strong reduction of surface elevation seen for all phases in Fig. 25 when moving upstream. From a maximum elevation of over 2 m at the mouth of the James River, the maximum elevation reduces to about 0.9-1.0 m up the river.

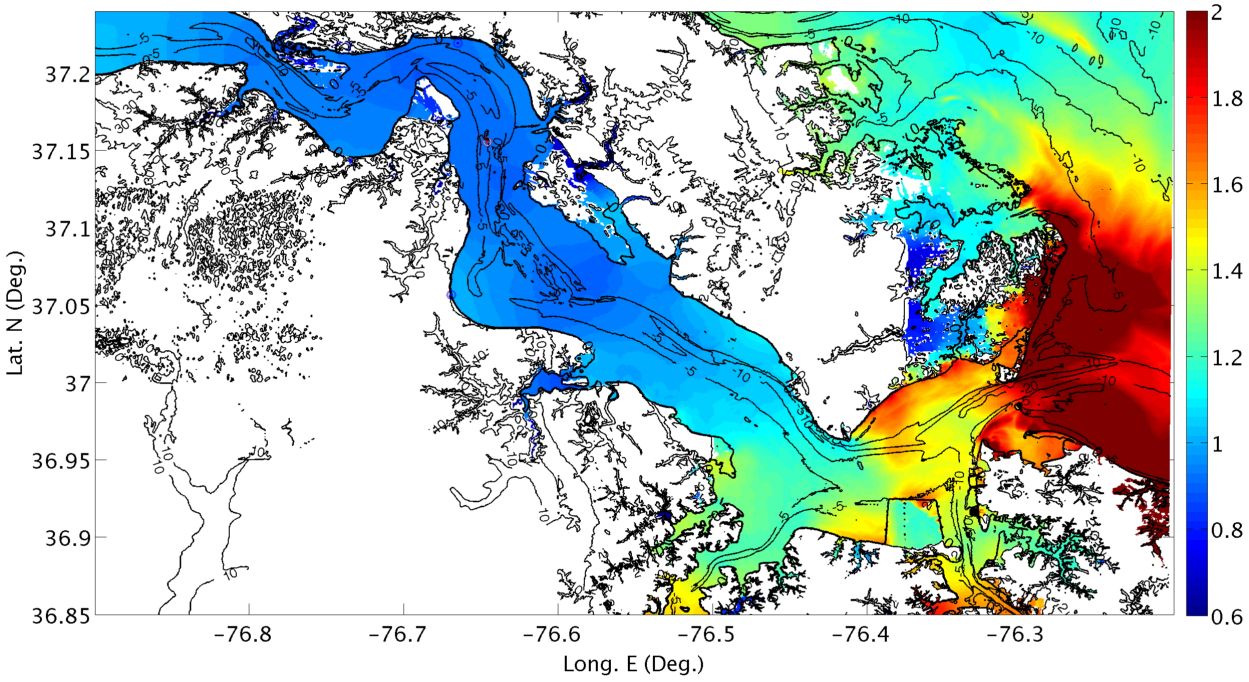

Fig. 28: Simulation with FUNWAVE-TVD (MHW+SLR reference level) of the calibrated M2 tide plus CRT tsunami. Envelope of maximum surface elevation (colorbar in meter) computed in 39 m grid for all tide phases (TT1, TT2, TT3 and TT4).

6. Conclusions

We conducted numerical simulations in a series of nested grids (up to 4 levels of nesting) that combined incident tsunami wave trains off the mouth of the Chesapeake Bay (2 extreme tsunami sources: one near-field Currituck SMF and one far-field CVV sources), plus the forcing from the M2 extreme tide for four phases of the tide.

The M2 tide was first calibrated from the mean values that were obtained from an independent model, by running simulations for the tide alone, to achieve the expected maximum antecedent water level (AWL) at the reference station of Sewells Pt (+0.957 m, MHW), near the mouth of the James River. In view of the observed reduction of modeled tide elevations, when going up the river to the locations of other tidal gages, these simulations revealed that, to match the expected reduction in tide elevation from Sewells Pt to upstream the James River, the relevant reference level in the model ought to be MHW, to which a sea level rise (SLR) value was added, yielding the actual mean water level in the tide plus tsunami simulations as MHW+SLR.

Simulations were then conducted for the 2 tsunamis, either alone over the static AWL, or combined with various phases of the tide. We first combined tide and tsunamis for the two maximum elevations to be synchronized at the mouth of the Chesapeake Bay. We then used a reduced tide elevation but maximum ebb current in the river (in order to cause tsunami shoaling) when the tide lags by one eight of its period (T/8) after the maximum tide (TT2) and when tide lags by T/4 after the maximum, downward zero crossing (TT3). As a last tide phase we used T/8 ahead of the maximum tide (TT4). To assess the effects of a these dynamic tide-tsunami simulations, we compared results of surface elevation and currents computed for various tide phases in the James River, to those obtained for both tsunamis when considering a static reference level equal to the maximum AWL at Sewells Pt, as recommended by the Nuclear Regulatory Commission (NRC) for performing tsunami hazard assessment at open ocean sites.

Based on these simulations, it appears that among the two tsunami sources and 4 tested phases of the tide, the worst-case scenario, leading to maximum inundation and currents in the James River, is the tsunami resulting from an extreme flank failure (450 km^3) of the Cumbre Vieja Volcano for the tide case TT4; for CVV, the tide phase case TT1, which synchronizes maximum tsunami with the maximum tide also causes nearly the same flooding at the mouth of the bay and in the James River. Other cases TT2 and TT3 cause less inundation and currents in the James River. For the latter CVV case (TT4), the inundation upstream the river near station #4 reaches 1.2 m above MHW+SLR reference level, or +1.686 NAVD88, which is +0.44 m above the Sewells Pt AWL. The tsunami resulting from such an event would take approximately 8 hours to travel across the Atlantic Ocean to the continental shelf break and approximately another 6.5 additional hours to travel from the shelf break to station #4, upstream the river.

Results for the CRT tsunami, although predicting a smaller impact, show that the maximum inundation at station #4 would be within 0.1 m of that of CVV and currents only 5 cm/s slower, when synchronized with the maximum tide elevation (TT1 case, unlike the maximum level for CVV, which occurs for the TT4 case). Hence, CRT results for cases TT1 and/or TT4 are also nearly worst-case scenarios for the James River; while CRT is not the absolute Probable Maximum Tsunami (PMT) expected for the upper US East coast (Grilli et al., 2015), it is still the near-field PMT for the Chesapeake Bay and James River areas. Because it is in the near-field,

this SMF tsunami would offer less time for warning (only a couple of hours to the mouth of the Bay and 4.5 hours to the upper part of the river) than the distant CVV source and, hence, may pose a greater hazard. As a mitigating factor, however, this SMF, if it occurred as a repeat of the historical Currituck slide, would likely be triggered by a large regional earthquake that would be very quickly felt in the area of the James River

In both the CVV and CRT cases, the standard simulation in tsunami hazard assessment recommended by NRC, of each tsunami over the maximum static AWL still produces conservative results in terms of maximum predicted inundation, at both station #2 and #4, but not by a large margin as compared to tsunami-tide interaction cases TT1 to TT4. Also, for cases TT1 and TT4, the duration of maximum inundation is longer and levels reached for subsequent waves in the tsunami wave-train higher than those obtained in the tsunami alone simulations (CVVSL, CRTSL). Clearly, such conclusions are case and site specific and, for river estuaries with stronger tidal currents than the order one-knot that occur in the James River, these conclusions could be reversed.

Various detailed results presented for both surface elevation and current time series in the river show that there are significant interactions of the tide induced current with the leading tsunami wave, but also in some cases with the second and third waves in the tsunami train, while these are propagating up the James River. Therefore, depending on the arrival time of tsunami waves with respect to the tide phase, the major flooding risk might result from different crests in the tsunami incident wave train and the arrival time of maximum flooding at a given gage may vary. This indicates that for tsunami event lasting hours, one should not downgrade the level of warning too soon since higher flooding and currents may occurs hours after the leading wave has arrived. Also, for tsunamis occurring at different phases of the tide, nonlinear interactions change the velocity of propagation of the various waves of the incident wave train in the shallower water area of the river. This can be seen in the time lag between the maximum elevation at Sewells Pt. and station # 4, which is not constant in different scenarios. Finally, the wave period at each station changes based on the phase of the tide, which is another sign of nonlinear interactions.

Acknowledgment

Partial funding for this work was provided by grant #NA14NWS4670041 of the National Tsunami Hazards Mitigation Program (NTHMP). RPS-ASC Inc. (Wakefield, RI) is acknowledged for providing us with the unscaled M2 tide forcing computed along the boundary of our 154 m grid result, and also for computing the antecedent water level at Sewells Pt., VA.

7. References

Abadie S., Harris J.C., Grilli S.T. and R. Fabre 2012. Numerical modeling of tsunami waves generated by the flank collapse of the Cumbre Vieja Volcano (La Palma, Canary Islands): tsunami source and near field effects. *J. Geophys. Res.*, **117**, C05030, doi:10.1029/2011JC007646.

Dean R.G. and R.A. Dalrymple 1990. *Water wave mechanics for engineers and scientists*. World Scientific Pub. (2nd edition), Singapore.

Egbert G.D., Bennett A.F., and M.G.G. Foreman 1994. TOPEX/POSEIDON tides estimated using a global inverse model. *J. Geophys. Res*., **99**(C12), 24821–24852.

Egbert G.D. and S.Y. Erofeeva 2002. Efficient Inverse Modeling of Barotropic Ocean Tides. *J. Atmos. Oceanic Technol*., **19**, 183–204

Enet F. and S.T. Grilli 2007. Experimental Study of Tsunami Generation by Three-dimensional Rigid Underwater Landslides. *Journal of Waterway Port Coastal and Ocean Engineering*, **133**(6), 442-454.

Grilli A.R. and S.T. Grilli 2013a. Modeling of tsunami generation, propagation and regional impact along the upper US east coast from the Puerto Rico trench. *Research Report no.* **CACR-13-02**. NTHMP Award, #NA10NWS4670010, National Weather Service Program Office, 18 pps.

Grilli A.R. and S.T. Grilli 2013b. Far-Field tsunami impact on the U.S. East Coast from an extreme flank collapse of the Cumbre Vieja Volcano (Canary Island). *Research Report no.* **CACR-13-03**. NTHMP Award, #NA10NWS4670010, National Weather Service Program Office, 13 pps.

Grilli A.R. and S.T. Grilli 2013c. Modeling of tsunami generation, propagation and regional impact along the U.S. East Coast from the Azores Convergence Zone. *Research Report no.* **CACR-13-04**. NTHMP Award, #NA10NWS4670010, National Weather Service Program Office, 20 pps.

Grilli S.T. and P. Watts 2005. Tsunami generation by submarine mass failure Part I : Modeling, experimental validation, and sensitivity analysis. *J. Waterway Port Coastal and Ocean Engng.,* 131(6), 283-297.

Grilli S.T., Ioualalen, M., Asavanant, J., Shi, F., Kirby, J. and Watts, P. 2007. Source Constraints and Model Simulation of the December 26, 2004 Indian Ocean Tsunami. *Journal of Waterway Port Coastal and Ocean Engineering*, **133**(6), 414-428.

Grilli S.T., Taylor, O.-D. S., Baxter, D.P. and S. Maretzki 2009. Probabilistic approach for determining submarine landslide tsunami hazard along the upper East Coast of the United States. *Marine Geology*, **264**(1-2), 74-97, doi:10.1016/j.margeo.2009.02.010.

Grilli S.T., Dubosq S., Pophet N., Pérignon Y., Kirby J.T. and F. Shi 2010. Numerical simulation and first-order hazard analysis of large co-seismic tsunamis generated in the Puerto Rico trench: near-field impact on the North shore of Puerto Rico and far-field impact on the US East Coast. *Natural Hazards and Earth System Sciences*, **10**, 2109-2125, doi:10.5194/nhess-2109-2010.

Grilli S.T., Harris J.C., Tajalibakhsh T., Masterlark T.L., Kyriakopoulos C., Kirby J.T. and F. Shi, 2013a. Numerical simulation of the 2011 Tohoku tsunami based on a new transient FEM co-seismic source: Comparison to far- and near-field observations *Pure and Applied Geophysics*, **170**, 1333-1359, doi:10.1007/s00024-012-0528-y (published online 7/24/12).

Grilli S.T., O'Reilly C. and T. Tajalli-Bakhsh 2013b. Modeling of SMF tsunami generation and regional impact alng the upper U.S. East Coast. *Research Report no.* **CACR-13-05**. NTHMP Award, #NA10NWS4670010, National Weather Service Program Office, 46 pps..

Grilli S.T., O'Reilly C., Harris J.C., Tajalli-Bakhsh T., Tehranirad B., Banihashemi S., Kirby J.T., Baxter C.D.P., Eggeling T., Ma G. and F. Shi 2015. Modeling of SMF tsunami hazard along the upper US East Coast: Detailed impact around Ocean City, MD. *Natural Hazards*, **76**(2), 705-746, doi: 10.1007/s11069-014-1522-8.

Grilli, S.T. and P. Watts 2005. Tsunami generation by submarine mass failure Part I : Modeling, experimental validation, and sensitivity analysis. *J. Waterway Port Coastal and Ocean Engng.*, **131**(6), 283-297.

Ioualalen M., Asavanant J., Kaewbanjak N., Grilli S.T., Kirby J.T. and P. Watts 2007. Modeling the 26th December 2004 Indian Ocean tsunami: Case study of impact in Thailand. *J. Geophys. Res.*, **112**, C07024, doi:10.1029/2006JC003850.

Kirby J.T., Shi F., Tehranirad B., Harris J.C. and S.T. Grilli 2013. Dispersive tsunami waves in the ocean: Model equations and sensitivity to dispersion and Coriolis effects. *Ocean Modeling*, **62**, 39-55, doi:10.1016/j.ocemod.2012.11.009.

Kowalik Z., Proshutinsky T., and Proshutinsky A. 2006. Tide–tsunami interactions. *Science of Tsunami Hazards*. 24(4), 242- 256 .

Kowalik Z. and A. Proshutinsky 2010. Tsunami–tide interactions: A Cook Inlet case study. *Continental Shelf Res.*,**30**(6), 633–642.

Ma G., Shi F. and J.T. Kirby 2012. Shock-capturing non-hydrostatic model for fully dispersive surface wave processes. *Ocean Modelling***, 43-44**, 22-35.

NOAA-NGDC (2013). National Geophysical Data Center, U.S. Coastal Relief Model, Retrieved December 2013, http://www.ngdc.noaa.gov/mgg/coastal/crm.html.

Shi F., Kirby J.T., Harris J.C., Geiman J.D. and S.T. Grilli 2012a. A High-Order Adaptive Time-Stepping TVD Solver for Boussinesq Modeling of Breaking Waves and Coastal Inundation. *Ocean Modeling*, **43-44**, 36-51, doi:10.1016/j.ocemod.2011.12.004.

Shi, F., Kirby, J. T. and Tehranirad, B. 2012b. Tsunami benchmark results for spherical coordinate version of FUNWAVE-TVD (Version 1.1). *Research Report No.* **CACR-12-02**, Center for Applied Coastal Research, Univ. of Delaware, Newark.

Taylor L.A., Eakins B.W., Carignan K.S., Warnken R.R., Sazonova T., Schoolcraft D.C. and G.F. Sharman 2008. Digital Elevation Model of Virginia Beach, Virginia: Procedures, Data Sources and Analysis, NOAA Technical Memorandum NESDIS NGDC-7, National Geophysical Data Center, Boulder, CO, 34 pp. http://ngdc.noaa.gov/dem/squareCellGrid/download/423.

Tehranirad B., Harris J.C., Grilli A.R., Grilli S.T., Abadie S., Kirby J.T. and F. Shi 2015. Far-field tsunami impact in the north Atlantic basin from large scale flank collapses of the Cumbre Vieja volcano, La Palma. *Pure and Applied Geophysics*, 28pps. doi:10.1007/s00024-015-1135-5 (published online 07/21/15).

Tehranirad B., Shi F., Kirby J.T., Harris J.C. and S.T. Grilli 2011. Tsunami benchmark results for fully nonlinear Boussinesq wave model FUNWAVE-TVD (Version) 1.0. *Research Report No.* **CACR-11-02**, Center for Applied Coastal Research, Univ. of Delaware, Newark.

Tehranirad B., Kirby J.T., Ma, G. and F. ShI 2012. Tsunami benchmark results for non-hydrostatic wave model NHWAVE (Version 1.0). *Research Report No.* **CACR-12-03**, Center for Applied Coastal Research, Univ. of Delaware, Newark.

ten Brink U.S., Twitchell D., Geist E., Chaytor J., Locat J., Lee H., Buczkowski B., Barkan R., Solow A., Andrews B., Parsons T., Lynett P., Lin J., and M. Sansoucy 2008. *Evaluation of tsunami sources with the potential to impact the U.S. Atlantic and Gulf Coasts*. Report to the Nuclear Regulatory Commission. USGS. 322 pp.

ten Brink U.S., Chaytor J.D., Geist E.L., Brothers D.S. and B.D. Andrews 2014. Assessment of tsunami hazard to the U.S. Atlantic margin. *Marine Geology*, **353**, 31-54.

Tolkova, E. 2012. Tide-tsunami interaction in Columbia River, as implied by historical data and numerical simulations. *Pure and Applied Geophysics*, **170**(6-8), 1115-1126.

Yeh H., Tolkova E., Jay D., Talke S. and H. Fritz 2012. Tsunami Hydrodynamics in the Columbia River. *J. Disaster Res.*, **7**(5), 604-608.

Ward S.N. and S. Day 2001. Cumbre Vieja Volcano – potential collapse and tsunami at La Palma, Canary Islands. *Geophys. Res. Lett.*, **21**, 397-400.

Wei J., Kirby J.T, Grilli S.T. and R. Subramanya 1995. A Fully Nonlinear Boussinesq Model for Surface Waves. Part1. Highly Nonlinear Unsteady Waves. *J. Fluid Mech.,* **294**, 71-92.

Zhang Y., Witter R.C. and G.R. Priest 2011. Tsunami–tide interaction in 1964 Prince William Sound tsunami. *Ocean Modelling*, **40**, 246–259.